Bactericidal Surfaces: An Emerging 21st Century Ultra-Precision Manufacturing and Materials Puzzle

3 **Mikel Larrañaga-Altuna[a,b], Alaitz Zabala[b], Iñigo Llavori[b], Oliver Pearce[c], Dinh T Nguyen[d],**

4 **Jaume Caro[e], Holger Mescheder[f], Jose L Endrino[g,h], Gaurav Goel[a,i], Wayne Nishio Ayre[j],**

5 **Rajkumar Kottayasamy Seenivasagam[k], Debendra Kumar Tripathy[k], Joe Armstrong[l] and**

6 **Saurav Goel[a,i,m*]**

7 [a] School of Aerospace, Transport and Manufacturing, Cranfield University, Bedfordshire,

8 MK43 0AL, UK

9 [b] Mechanical and Industrial Manufacturing Department, Mondragon Unibertsitatea,

10 Loramendi 4, 20500, Mondragón, Spain

11 [c] Orthopaedic Department, Milton Keynes University Hospital, MK65 LD, UK

12 [d] Multitel ABSL, Rue Pierre et Marie Curie 2, Mons, 7000, Belgium

13 [e] Eurecat, Centre Tecnològic de Catalunya, Unit of Metallic and Ceramic Materials, Plaça

14 de la Ciència 2, 08243 Manresa, Spain.

15 [f] Fraunhofer-Institut für Produktionstechnologie, IPT, 52074, Aachen, Germany

16 [g] Basque Center for Materials, Applications & Nanostructures, UPV/EHU Science Park,

17 Barrio Sarriena s/n, 48940 Leioa, Spain.

18 [h] IKERBASQUE, Basque Foundation for Science, Maria Diaz de Haro 3, 48013 Bilbao,

19 Spain.

20 [i] School of Engineering, London South Bank University, 103 Borough Road, London,

21 SE1 0AA, UK

22 [j] School of Dentistry, Cardiff University, Heath Park, Cardiff, CF14 4XY

23 [k] All India Institute of Medical Sciences Rishikesh, India

24 [l] Polytec GmbH, Polytec-Platz 1-7 76337 Waldbronn, Germany

25 [m] Department of Mechanical Engineering, Shiv Nadar University, Gautam Budh Nagar,

26 201314, India

27 * Corresponding Author email: GoeLs@LSBU.ac.uk

28 **Abstract**

29 Progress made by materials scientists in recent years has greatly helped the field of ultra-
30 precision manufacturing. Ranging from healthcare to electronics components,
31 phenomena such as twinning, dislocation nucleation and high-pressure phase
32 transformation have helped to exploit plasticity across a wide range of metallic and
33 semiconductor materials. One current problem at the forefront of the healthcare sector
34 that can benefit from these advances is that of bacterial infections in implanted prosthetic
35 devices. The treatment of implant infections is often complicated by the growth of
36 bacterial biofilms on implant surfaces, which form a barrier that effectively protects the
37 infecting organisms from host immune defences and exogenous antibiotics. Further
38 surgery is usually required to disrupt the biofilm, or to remove the implant altogether to
39 permit antibiotics to clear the infection, incurring considerable cost and healthcare
40 burdens. In this review, we focus on elucidating aspects of bactericidal surfaces inspired
41 by the biological world to inform the design of implant surface treatments that will
42 suppress bacterial colonization. Alongside manufacturing and materials related
43 challenges, the review identifies the most promising natural bactericidal surfaces and
44 provides representative models of their structure, highlighting the importance of the
45 critical slope presented by these surfaces. The scalable production of these complex
46 hierarchical structures on freeform metallic implant surfaces has remained a scientific
47 challenge to date and as identified by this review, is one of the many 21st Century puzzles
48 to be addressed by the field of applied physics.

49

51

52

53

54

55

56

57

94

95   **Abbreviations**

96   AFM: Atomic Force Microscope

97   CA: Contact Angle

98   CAD: Computer-Aided Design

99   CAH: Contact Angle Hysteresis

100   CNC: Computer Numerical Control

101   CVD: Chemical Vapour Deposition

102   ECAP: Equal Channel Angular Pressing

103   ED: Emergency department

104   EDM: Electro Discharge Machining

105   EDS: Energy-Dispersive Spectroscopy

106   EPS: Extracellular Polymeric Substance

107   NHS: National Health Service

108   PDMSe: Dimethylpolysiloxane

109   PPI: Plasma Immersion Ion Implantation

110   SEM: Scanning Electron Microscopy

111   TEM: Transmission Electron Microscope

112   UK: United Kingdom

113   UPM: Ultra Precision Manufacturing

114   USA: United States of America

115

116   **Nomenclatures**

117   θ: Contact angle

118   γ_{sv}: Surface tension between the solid phase and vapour phase

119   γ_{sl}: Surface tension between the solid phase and liquid phase

120   γ_{lv}: Surface tension between the liquid solid phase.

121   r: Roughness parameter

122   θ_A: Apparent contact angle

123   θ_Y: Young's contact angle

124   f_1: Fraction of solid material in contact with liquid

125   f_2: Fraction of air in contact with the liquid

126   θ_1: Contact angle of the solid material

127   Ø: Diameter

128   R_a: Arithmetical mean deviation of the assessed profile

129

130

1. Introduction

Biohazards and biothreats are becoming more ubiquitous than before[1]. One of the forefront issues in healthcare is how to avoid repeated surgeries due to implant failure. If one reviews the total lifecycle of an implant, it becomes clear that the challenges faced span fields of materials science[2] (selection of material to avoid stress shielding and ensure biocompatibility), manufacturing (fabrication to obtain the compliant shape by subtractive or additive manufacturing routes) and biological sciences (promoting osseointegration and avoiding biofilm formation and bacterial infection).

Despite processes such as sterilisation and even use of antimicrobial coatings, a risk exists of the implant surface being susceptible to bacterial infection at any point of time during its service life. Clinical evidence suggests that numerous species of bacteria are implicated in the infection of medical implants. The most common pathogens identified are *Staphylococcus aureus*[3], *Escherichia coli*, *Proteus mirabilis* and *Pseudomonas aeruginosa*[4]. Treating these bacteria with antibiotics alone is often ineffective as *in vivo* they surround themselves by an active matrix of cells and extracellular substances consisting of glucose [5] (glycocalyx shell) formed on the implant surface, which is impermeable to drugs or antibiotics[6]. As a result, an infected implant usually requires further surgery as part of its treatment. This carries operative and anaesthetic risks and a prolonged period of antibiotic treatment thereafter (around 3 months). It is estimated that about 2000 cases of hip and knee replacements become infected every year[7] in the UK alone. Joint replacements are not the only implanted devices in the human body; however, they are one of the most widely studied. Other implants where infections pose a significant risk include vascular stents, cardiac pacemakers, fracture fixation plates and nails, dental implants, nerve stimulators, cochlear implants, and many more. To address this issue of infection, several different approaches have been proposed: from antibiotic coatings[8] to surface modifications[9] that prevent bacterial adhesion and suppress the proliferation of bacteria.

Nature has become a great inspiration for materials scientists and engineers due to the presence of effective antimicrobial materials with micro and nanostructures, which evolved over millions of years. These hierarchical structures are found mainly in the lotus leaf, gecko skin, dragonfly wings or cicada wings[10], among others, giving extraordinary surface properties, such as superhydrophobicity[11], adhesion[12], antibiofouling[13] or bactericidal activity[14].

164   Scientists have made collective efforts in order to understand and mimic these
165   extraordinary surfaces, termed nature-inspired surfaces. This is the reason why nature can
166   be considered as the best laboratory for inspiring us to understand hierarchical structures
167   or put simply "patterned surfaces". Over the last decade, understanding of micro- and
168   nanometre scale surfaces has played an important role in improving our knowledge of
169   how some of the surfaces seen in nature possess unique properties. For example, it has
170   been reported that the dragonfly wing nanostructure is able to kill either Gram-positive
171   (which have a thick peptidoglycan layer) or Gram-negative bacteria (which have a thinner
172   peptidoglycan layer with an additional negatively charged lipopolysaccharide layer)
173   [10,15,16]. As such, bacterial adhesion has been widely modelled by the DLVO (Derjaguin,
174   Landau, Verwey and Overbeek) theory which is governed by van der Waals forces[17] and
175   by various surface properties such as topography, chemical composition, or morphology
176   of the surface[14,18] which are discussed at length in the later section of this paper. Adhesion
177   is also governed by surface conditioning blood proteins, such as fibronectin, fibrinogen
178   and vitronectin, other molecules such as von Willebrand factor and polysaccharides [5]. *S.*
179   *aureus,* widely implicated in infection of numerous medical devices, expresses two
180   fibronectin binding proteins (FnBPA and FnBPB), which as the name suggests, facilitates
181   binding to fibronectin on implant surfaces[19]. Similarly, *S. epidermidis*, another pathogen
182   associated with joint replacement infections expresses surface associated autolysin
183   (At1E), which encourages binding to polymeric surfaces[5]. Other mechanisms of adhesion
184   include modulation of fimbriae and polysaccharide adhesins, often associated with Gram-
185   negative bacteria[20].

186   The shift from a planktonic (free-floating) to a sessile (attached) state induces expression
187   of several genes responsible for production of extracellular polymeric substance (EPS),
188   resulting in the formation of a biofilm. Both Gram-positive and Gram-negative bacteria
189   can form biofilms on medical devices; most common of which are *Enterococcus faecalis,*
190   *S. aureus, S. epidermidis* and *Streptococcus viridans* (Gram-positive) and *E. coli,*
191   *Klebsiella pneumoniae, Proteus mirabilis* and *P. aeruginosa* (Gram-negative bacteria)[21].

192   Biofilms consist predominantly of a mixture of polysaccharides, nucleic acids
193   (extracellular DNA or eDNA), proteins (composed primarily of D-amino acids) and fatty
194   acids[22]. Extracellular DNA plays a key role in cellular communication in early stages of
195   biofilm development and is modulated by quorum sensing, a density-dependent
196   phenomenon that controls gene expression. *In vivo*, biofilms are often encountered as

197 mixed species with composition of the biofilm varying depending on the species of

198 bacteria present and the properties of the underlying surface. *P. aeruginosa* releases three

199 polysaccharides (alginate, Pel and Psl) which provides mechanical stability;

200 staphylococci produce polysaccharide intercellular adhesin (PIA) that allows it to form

201 biofilms specifically on orthopaedic biomaterials; and more broadly for quorum sensing,

202 Gram-negative bacteria release acyl-homoserine lactones, whereas Gram- positive

203 bacteria release peptide molecules[22].

204 The differences in biofilm composition and species present plays an important role in

205 pathogenicity and virulence of the infection. As previously mentioned, staphylococci

206 biofilms are often associated with orthopaedic implants, whilst dental implant biofilms

207 consist of a mixed sequential attachment of early colonisers (e.g. *Aggregatibacter*

208 *actinomycetemcomitans),* followed by bridging species (e.g. *Fusobacterium nucleatum*)

209 and finally more pathogenic bacteria (e.g. *Porphyromonas gingivalis*)[23]. Catheter

210 associated infections are associated with *Proteus mirabilis* biofilms, which results in a

211 rise in pH and subsequent crystallisation of minerals and catheter blockage[24].

212 Nevertheless, all biofilms follow three classical stages: initial attachment (reversible and

213 irreversible), maturation and detachment/dispersal, with the main role of the biofilm

214 being to protect the bacteria from the host defence system or from external agents such

215 as antibiotics. It is reported that bacteria in biofilms are 500–5000 times more tolerant

216 towards antibiotics[25] and therefore non-antibiotic approaches to inhibit initial attachment

217 and biofilm formation are clearly needed. By controlling surface properties, the

218 bactericidal efficacy of medical devices such as implants or surgical tools may be

219 improved. Thus, an improved understanding of the bacteria-surface interaction is an

220 important step towards the design of an anti-infective medical implant.

221 Fabrication of bio-inspired patterned surfaces, however, requires analysis and design of

222 these complex geometries to be reproduced accurately with surface modification methods

223 currently available. An emerging new branch of manufacturing called 'Ultra Precision

224 Manufacturing' has helped in developing fabrication solutions such as machine tools and

225 processing technologies required for fabricating nanostructured precision surfaces with

226 great repeatability and accuracy. This manuscript is targeted at consolidating a deeper

227 understanding of nature-inspired patterned surfaces and to understand the challenges in

228 fabricating these precise surfaces on somewhat difficult to cut materials, such as CoCr,

229 Ti6Al4V and stainless-steel alloys, which are amongst the most popular medical implant
230 materials used.

231 In this paper, the focus is on salient aspects of 'nature-inspired surfaces', primarily
232 applicable to implants. Considering this, some CAD models are proposed according to
233 reviewed literature to facilitate future manufacturing. Moreover, the main surface effects
234 such as topography, wettability or chemistry are discussed to shed light on how to prevent
235 bacterial adhesion. Finally, the prominent fabrication routes for surface patterning are
236 briefly reviewed. Figure 1 summarises the structure and content of this interdisciplinary
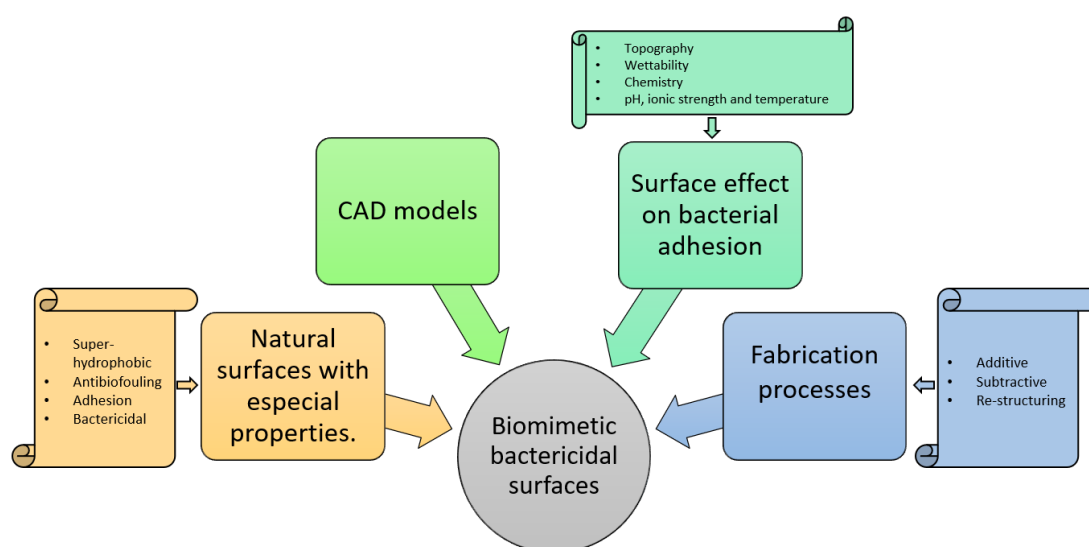237 review article.

238

239 Figure 1: Schematic representation of the various aspects discussed in this review paper.

240 **2. Review of nature inspired bactericidal surfaces**

241 *2.1 Science of wettability*

242 Wetting is the ability of a liquid to maintain contact with a solid surface[26]. Wettability
243 plays an important role in ensuring the desired biological response of biomaterials.
244 Surface wettability may influence adhesion and growth of bacteria on biomaterials and in
245 some cases, it is the dominant factor such as in attachment of *S. epidermidis* on titanium
246 and zirconium dental implants.

247 Measurement of wettability or in turn the contact angle of a liquid droplet is currently
248 used as an indirect measurement of cellular activity on the surface. However, the exact
249 effect of surface wettability on bacterial adhesion or growth is yet to be established.
250 Wettability is largely governed by surface topography (roughness and morphology) and

251   chemical composition (surface energy)[27]. Control of these surface properties has received

252   much interest in a wide range of applications ranging from aerospace, healthcare and

253   agriculture[28]. Contact angle (θ), is the most widely used indicator to quantify wettability

254   and is determined by calculating the angle between the tangent to liquid-air interface and

255   the line that represents solid-liquid interface. Depending on the contact angle value, a

256   surface may be divided into four main categories[27] as shown in Table I. Different wetting

257   models have been developed to describe the wetting of smooth (Young's) and patterned

258   surfaces (Wenzel's and Cassie-Baxter's equations) as shown in Figure 2. These models

259   are very important in studying wettability as they can be used for determining contact

260   angles on different surfaces which in turn defines biological behaviour of materials.

261   Table I: Type of surface depending on the CA

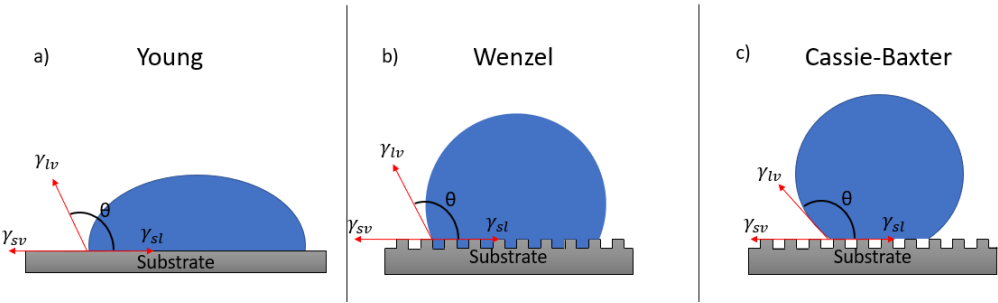| Type of surface	Contact angle (CA)
Superhydrophobic	CA>150°
Hydrophobic	150°>CA>90°
Hydrophilic	90°>CA>10°
Superhydrophilic	CA<10°

262

264   Figure 2: Models used to measure the contact angle of the surface. a) Young, b) Wenzel

265   and c) Cassie-Baxter model

266   *2.1.1   Hierarchical structures*

267   Hierarchical structures present a combination of structures at multiple levels (Figure 3),

268   varying from micro to nano level[29] and can be regarded as composite structures exhibiting

269   features at multiple length scales. They are responsible for non-wetting superhydrophobic

270   properties of natural surfaces which have been intensively studied as an inspiration for

271   designing and fabricating artificial surfaces used in biomedical applications[13].
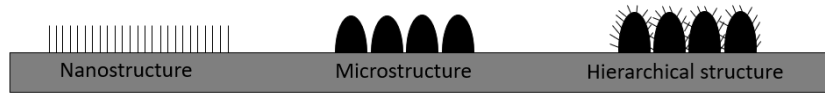
272

273   Figure 3: Different levels of structures, from nanostructures to hierarchical structures

274   Such surface structures are quite commonly found in plants[30] as well as on animal skin[31].

275   The most common morphologies found in plants present one convex shape that creates

276   the base at the micron level, whereas at the nano-level a cuticular folding is found[29]. The

277   main advantage of these types of structures is that they can create air pockets, leading to

278   the lowest contact area between the surface and water drop, thus presenting an increased

279   contact angle. Figure 4 shows an example of different surface structures and a comparison

280   between contact angles. Koch *et al.*[30] concluded from their investigation that hierarchical

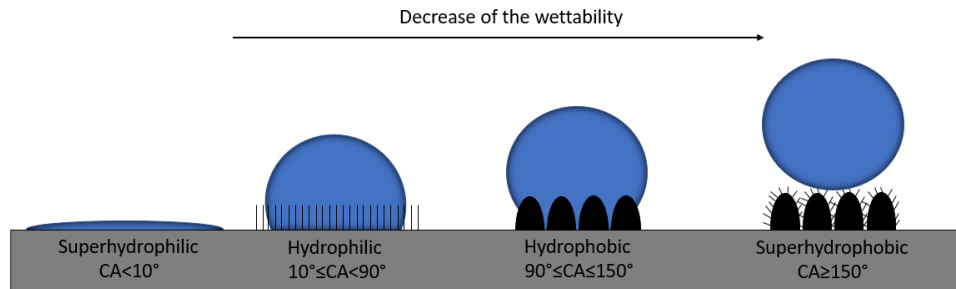281   structures are responsible for superhydrophobicity in most plants.

282

283   Figure 4: Different surface structures, starting smooth surface (left), nanostructure,

284   microstructure and hierarchical structure (right). Reproduced with permission from J. Soft

285   Matter 4, 1943 (2008), Copyright 2008, Royal Society of Chemistry[30]

286   *2.1.2   Young's model of wettability*

287   Young's model is used to describe wetting on ideally smooth, rigid, chemically

288   homogeneous, insoluble and non-reactive surfaces[14]. On these surfaces, the contact angle

289   (θ) depends on surface free energy and is calculated as:

$$\cos\theta = \frac{\gamma_{sv} - \gamma_{sl}}{\gamma_{lv}} \tag{1}$$

290   where, θ is Young's contact angle, γ_{sv} is surface tension between solid phase and vapour

291   phase, γ_{sl} between solid phase and liquid phase and γ_{lv} between liquid solid phase.

292   The Young's equation (1) is only valid for a flat and homogeneous surface with Young's

293   contact angle smaller than 120°. When surfaces are not considered ideally smooth, rigid

294   or chemically homogeneous, Young's models cannot be employed. For rough surfaces,

295   two different models have been developed to better describe the wettability about surface

296   roughness and surface energy and these are Wenzel and Cassie-Baxter models (shown

297   earlier in Figure 2b and Figure 2c) respectively.

298   *2.1.3   Wenzel model of wettability*

299   The Wenzel model describes the homogeneous wetting regime of textured surfaces[32]. It

300   means that a water drop sits on the surface, wetting the whole area (Figure 2b). The

301   contact angle for this case can be estimated as[33]:

$$cos\theta_A = rcos\theta_Y \tag{2}$$

302   where, θ_A is the apparent contact angle, θ_Y is Young's contact angle and r is the roughness

303   parameter, defined as projected area of the water droplet[14]. The Wenzel equation (2)

304   shows that for a rough surface, the apparent contact angle increases with increased surface

305   roughness. However, this relationship only holds with a surface roughness smaller or

306   equal to 1.7 µm ($r \leq 1.7$). If greater than that, the heterogeneous regime (described by

307   Cassie-Baxter's model) starts in which air is increasingly presented and trapped between

308   solid and water surfaces, resulting in a decrease of this angle.

309   *2.1.4   Cassie-Baxter model of wettability*

310   The Cassie-Baxter model describes the heterogeneous regime where the water drop does

311   not wet the whole surface due to air trapped between the rough surfaces (Figure 2c). For

312   this model, contact angle[34] may be calculated as:

$$cos\theta_A = f_1cos\theta_1 - f_2 \tag{3}$$

313   where, θ_A is the apparent contact angle, θ_1 is contact angle of solid material, f_1 is fraction

314   of solid material in contact with fluid, f_2 is fraction of air in contact with liquid. The

315   droplets in the Cassie-Baxter model provide a higher contact angle due to air trapped

316   between the surface and water drop[35]. Carbone et al.[36] reported an analytical model where

317   the transition from the Cassie-Baxter and Wenzel model has been calculated for rough

318   surfaces taking into account the applied pressure and height of the rough surface.

319   **2.2 Functionalities of selective nature-inspired patterned surfaces**

320   A wide range of natural surface functionalities has attracted scientists over the last few

321   decades due to their special properties. Sun and Bhushan[37] gathered the most studied

322   natural surfaces over the last 45 years starting from the superhydrophobic shark skin

323   property discovered in 1985 to the drag reduction property discovered in 2016. Figure 5

324   shows a few examples of natural functionalities and the most studied examples.
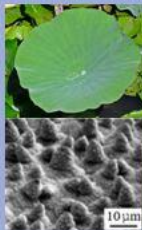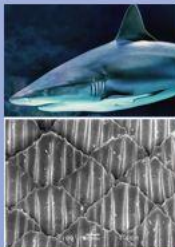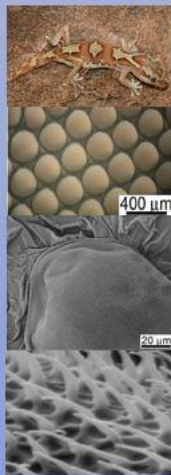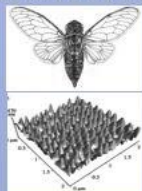
Figure 5: Functionalities of some of the nature inspired surfaces and some of their most studied properties.

1   *2.2.1   Superhydrophobicity*

2   The lotus leaf is known for its self-cleaning and superhydrophobic properties[13,38,39,40].

3   This extraordinary property relies on its randomly distributed 5 to 9 µm diameter

4   micropapillae covered by 120 nm in diameter and 200 to 400 nm long branch-like

5   nanostructures[11,31,41] shown in Figure 6.

6
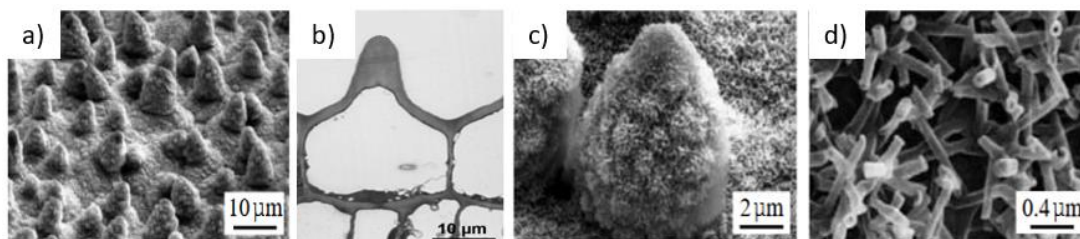
7   Figure 6: a) Microstructure of lotus leaf. Reproduced with permission from J. Soft Matter
8   5, 1386 (2009), Copyright 2009, Royal Society of Chemistry[42] b) Cross section of
9   micropapillae. Reproduced with permission from H.J. Ensikat, P. Ditsche-Kuru, C.
10   Neinhuis, and W. Barthlott, Beilstein J. Nanotechnol. **2**, 152 (2011), licensed under a
11   Creative Commons Attribution (CC BY) license [43] c) Micropapillae covered with
12   epicuticular waxes and d) branch like nanostructures. Reproduced with permission from
13   J. Soft Matter 5, 1386 (2009), Copyright 2009, Royal Society of Chemistry[42].
14

15   It should be noted that the lotus leaf microstructure is covered by epicuticular waxes

16   (made from hydrocarbon chains). The combination of hierarchical structure and the

17   waxes lead to improved contact angle of up to 164°[42]. Nishimoto *et al.*[39] reported that if

18   the superficial waxes are removed with acetone, the CA decreases dramatically and this

19   highlights the importance of surface chemistry alongside surface geometry. Besides, a

20   lotus leaf has a Contact Angle Hysteresis (CAH) of less than 5°[39]. For lower values of

21   CAH, the droplet may roll and slide on the surface[44]. The combination of

22   superhydrophobicity and low CAH provides a self-cleaning effect for the lotus leaf

23   (Figure 7).

24
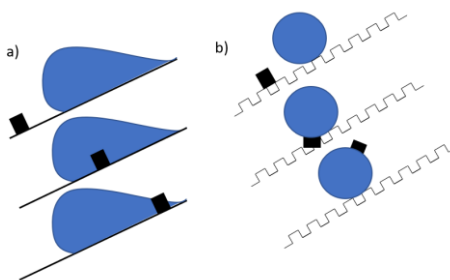
25   Figure 7: Schematic illustration of the lotus leaf self-cleaning effect a) ideal smooth

26   surfaces b) rough surfaces (black mark indicates a roll off point)

27   These properties make the lotus leaf an ideal bacterial repellent surface[45]. Fadeeva *et al.*[46]

28   used laser processing to mimic the lotus leaf hierarchical structures on titanium. They

29   reported a significant reduction in Gram-negative *P. aeruginosa* bacteria in comparison

30   to a polished surface. In contrast to this, an increase in Gram-positive *S. aureus* bacterial

31   adhesion was observed. Similar structures may be seen on the taro leaf, possessing

32   superhydrophobicity and self-cleaning abilities due to hierarchical structure[47]. The

33   microstructure of this surface consists of elliptical bumps, 10 µm to 30 µm in diameter,

34   covered by randomly distributed epicuticular waxes (Figure 8). Similar to a lotus leaf,

35   these waxes increase the contact angle of taro leaf from 90° to 150°[45].

36
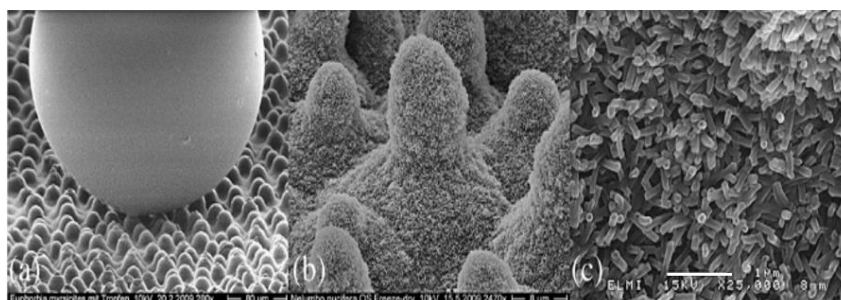
37   Figure 8: a) SEM image of the taro leaf with a water droplet showing the

38   superhydrophobic properties. b) Taro leaf bump-like microstructure and c) bumps

39   covered by epicuticular waxes. Scale bars are a) 80 µm b) 8 µm c) 1 µm. Reproduced

40   with permission from Adv. Colloid Interface Sci. **169**, 80 (2011)., Copyright 2011,

41   Elsevier [47].

42   Another example of a superhydrophobic surface is found on the *Morpho aega* butterfly

43   wing[31,48,49, 50,51,52]. The wings are not only superhydrophobic (CA of 152±2°[39]), but also

44   attractive to insects due to their chemical sensing capability or physical fluorescence

45   emission functions[39]. The microstructure of these wings consists of overlapped scales,

46   150 µm in length and 70 µm in width, where each scale consists of ridging nanostripes

47   184 nm in width with a 585 nm clearance [53]. Figure 9 shows the microstructure of *Morpho*

48   *aega* butterfly wings.

49

50
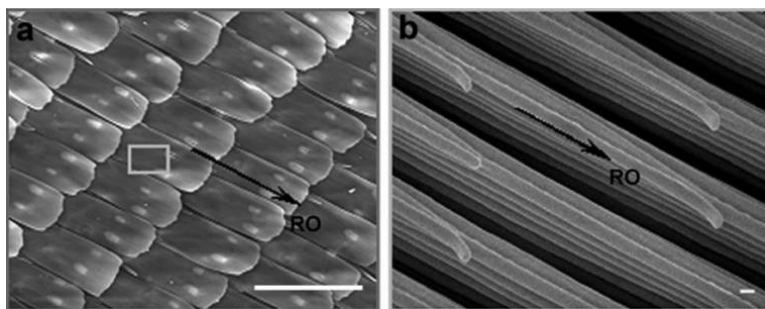
Figure 9: a) Butterfly wing scales, scale bar 100µm and b) nanostripes, scale bar 100 nm. Reproduced with permission from J. Soft Matter 3, 178 (2007), Copyright 2007, Royal Society of Chemistry[53].

2.2.2 Anti-biofouling

Shark skin is known to possess anti-biofouling, self-cleaning, hydrophobic and hydrodynamic properties evolved over millions of years[44]. These properties rely on a rhombus denticle based microstructures with five riblets 200 to 300 µm in length, 20 to 30 µm in height and 50 to 80 µm in width. Figure 10 shows a representation of shark skin microstructure, which helps a shark to swim fast[54].

60
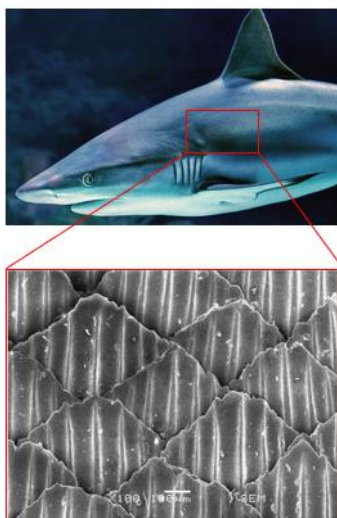
Figure 10: Shark skin riblet based microstructure. Scale bar 100 µm. Reproduced with permission from Mat Proc. Tech. 212, 198 (2012), Copyright 2012, Elsevier [54]

Due to these outstanding properties, different attempts have been carried out to mimic shark skin. Chung *et al*.[55] manufactured a PDMSe elastomer with Sharklet AF™ microstructure (Figure 11). Sharklet AF™ is known as the most successful design to replicate shark skin[56,57]. In their study, *S. aureus* bacteria was employed to test the bactericidal efficacy of this surface. After 31 days, the results showed a 42 % less covered

68   bacterial area on the structured surface compared to a smooth surface. Furthermore, no

69   biofilm formation was observed on the Sharklet AF™ surface.
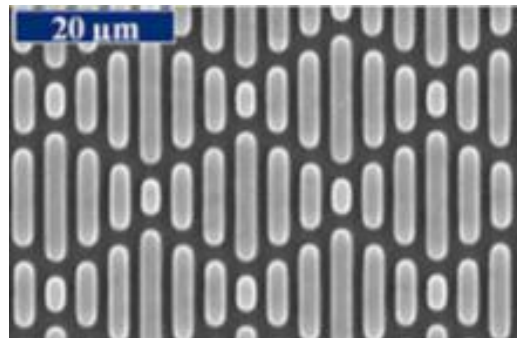
70

71   Figure 11: Scanning electron micrograph of the top view Sharklet AF™ microstructure.

72   Reproduced from BioInterphases 2, 89 (2007), with the permission of AIP Publishing[55].

73   *2.2.3   Adhesion*

74   Lots of insects and animals, such as flies, bees, and geckos, are well known for their

75   ability to stick onto a wide range of surfaces. Geckos are a particularly interesting species

76   because of high body mass and high density of terminal elements[31]. The detachment

77   mechanism of micropatterned natural surfaces (geckos included) has been widely

78   studied[58].

79   The hierarchical structure of the gecko foot consists of hundreds of setae varying from 30

80   µm to 130 µm long with each setae having hundreds of spatulae in sizes from 0.2 µm to

81   0.5 µm[31,59]. Figure 12 show details of the gecko's foot microstructure.
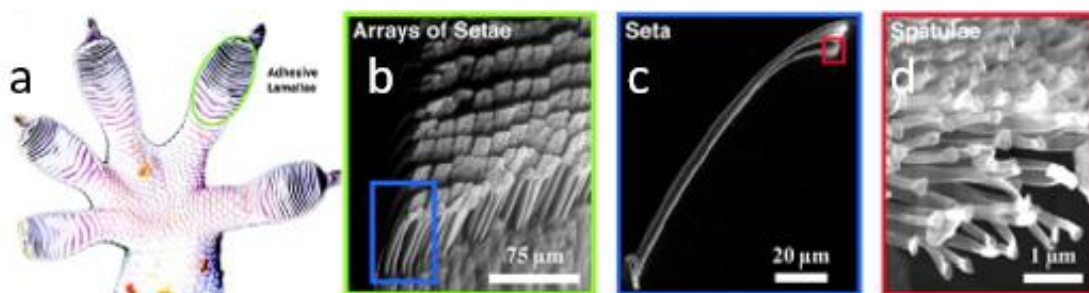
82

83   Figure 12: a) Gecko foot. b) Group of setae c) a single seta and d) Group of spatulas.

84   Reproduced with permission from Prog Nat Acad Sci, 102, 385 (2005), Copyright 2005,

85   US National Academy of Sciences[60].

86   It has been reported that gecko feet can generate a 10 N adhesive force per 10 mm^2 area[31].

87   Spatulae can tolerate higher load (several times the weight of the geckos) by van der

88   Waals forces.

89 The gecko's foot is not the only scientifically attractive part of this animal; the dorsal or

90 abdominal parts (Figure 13) also possess some advanced surface properties such as

91 antibacterial or self-cleaning[12,61] characteristics. The hierarchical structure of the gecko's

92 abdomen consists of 100 µm to 190 µm diameter scales (up to 300 µm for dorsal), 50 µm

93 in height (Figure 13c). Each scale is covered with hundreds of spinules, the length of

94 which varies from 0.5 µm to 1 µm with a 10 nm to 30 nm radius of curvature at their tip

95 (Figure 13e).

96
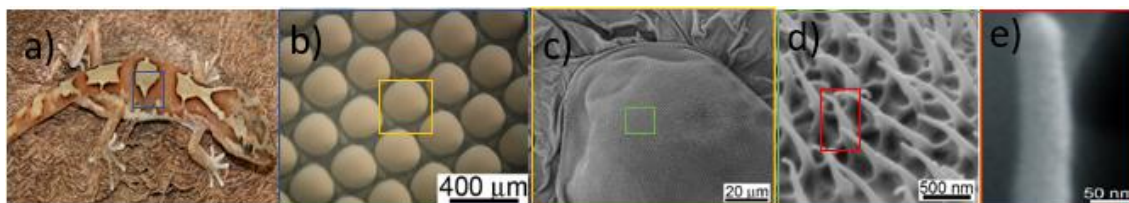
97 Figure 13: a) Lucasium steindachneri gecko b) Optical image of the abdominal part of

98 gecko c) Topographical SEM image of the scales. d) Group of spinules in the top of the

99 scales. e) magnification of the spinules at the nanometer scale. Reproduced with

100 permission from Acta BioMaterialia 21, 109 (2015), Copyright 2015, Elsevier [12].

101

102 Regarding the antibacterial and self-cleaning properties of the gecko dorsal and

103 abdominal dorsum, Watson et al.[12] carried out bacterial and self-cleaning experiments

104 where gecko dorsal skin was analysed. For the bacterial analysis, *P. gingivalis* bacteria

105 (associated with dental implant infections) were employed and for the self-cleaning

106 ability, water droplets were employed. They concluded that the gecko dorsal skin CA was

107 between 151° and 155° and was able to decrease *P. gingivalis* adhesion as well as having

108 a self-cleaning ability. Li et al.[62] also compared the adhesion of two different bacteria into

109 the dorsal dorsum of the gecko. They proposed a model for the interaction between Gram-

110 negative bacteria and the gecko skin. A mechanism that due to the stretching and

111 compression between the bacteria and gecko spinules causes bacterial rupture.

112 *2.2.4 Bactericidal surfaces*

113 Bactericidal surfaces are bacterial resistant surfaces capable of eliminating bacteria by

114 providing reduced contact area to thereby create tensile strain in the cell walls of the

115 bacteria causing it to rupture. There are many bactericidal surfaces reported, such as those

116 of the lotus leaf or gecko skin that due to the anti-biofouling or self-cleaning properties

117 may avoid the growth of bacterial adhesion[10,38,39,45]. Some insect wings have been

118   investigated due to their bactericidal properties, such as cicada and dragonfly wings,

119   which showed great promise for developing anti-infective surfaces[10,38,45].

120   Cicada wings are known to be bactericidal against *P. aeruginosa* and *S. cerevisiae*[10,38,63].

121   The nanostructure of the cicada wing consists of nanopillars with 200 nm height, 170 nm

122   spacing and 60 nm and 100 nm top and base diameters respectively[63]. Figure 14a shows

123   an Atomic Force Microscope (AFM) image of the cicada wing nanostructure. Moreover,

124   apart from being bactericidal surfaces, they are also known for superhydrophobicity, with

125   CA of 160 ° and self-cleaning properties[10].

126
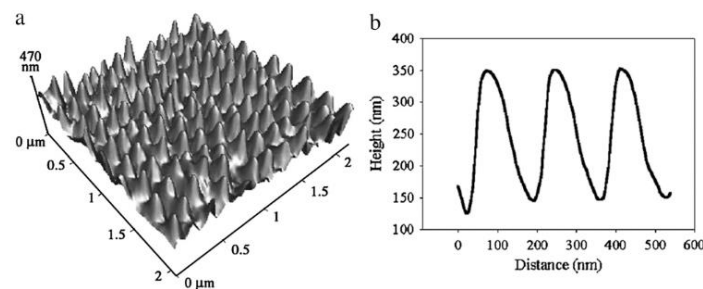
127   Figure 14: a) AFM three-dimensional image of a cicada wing and b) corresponding height

128   and width profile. Reproduced with permission from J. of BioPhysics 94, 3352 (2008),

129   Copyright 2008, Elsevier[64].

130   It should be noted that the anti-biofouling property of cicada wings does not lie in the

131   ability to repel the bacteria, but in its surface nanostructure and ability to kill the bacteria

132   by contact[10].

133   It was reported that the cicada wings were able to kill only Gram-negative bacteria[65]. This

134   was attributed to the wall thickness of a Gram-negative bacteria which is 4 or 5 times

135   thinner than Gram-positive bacteria[10]. Ivanova *et al.*[63] carried out an experiment where

136   *P. aeruginosa* bacteria were tested on the Cicada wings. It was observed that this surface

137   was able to effectively kill this bacterium.

138   To advance the understanding of the interaction between Gram-negative bacteria and the

139   cicada wing surface nanostructure, Pogodin *et al.*[66] developed a biophysical model. They

140   concluded that the region where the bacteria ruptured was between the pillars (Figure 15).

141   Specifically, it was not the intrusion of the structure into the substance of the bacterium

142   that punctures the bacterium, but a rupture of the membrane in the region between

143   adjacent spikes. Rupture of the bacterial membrane results in catastrophic leakage of the

144   cellular contents resulting in bacterial death.

145
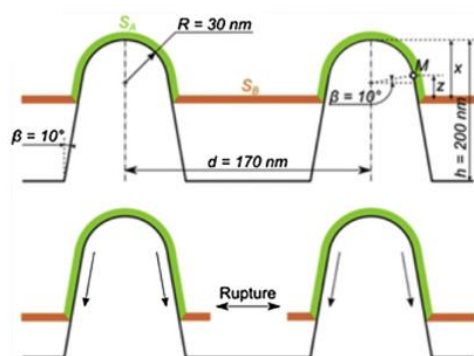
146   Figure 15: Model of cicada wing and bacteria explaining rupture of bacteria. Reproduced

147   with permission from J. of BioPhysics 104, 835 (2013), Copyright 2013, Elsevier[66].

148   A recent study by Román-Kustas et al.[67] shows that the bactericidal effect of the cicada

149   wings are not only attributed to the surface morphology but the chemical composition of

150   the surface also plays a key role in the bacterial rupture.

151   Another natural excellent bactericidal surface is found on dragonfly wings [45]. This surface

152   has a CA of $153°$[10]. The nanostructure of the dragonfly wing consists of randomly

153   distributed nanopillars with a variable diameter between 50 nm to 80 nm, 200 nm to 300

154   nm in height and 180 nm spacings between the pillars (Figure 16)[68]. In contrast to this,

155   Bandara et al.[15] analysed the topography of the dragonfly wing and identified two pillar

156   type structures; randomly distributed tall and short nanopillars. They reported a base

157   diameter of 37±6 nm and 57±8 nm for short and tall nanopillars respectively and 189±67

158   nm and 311 ±52 nm height for short and tall respectively.

159
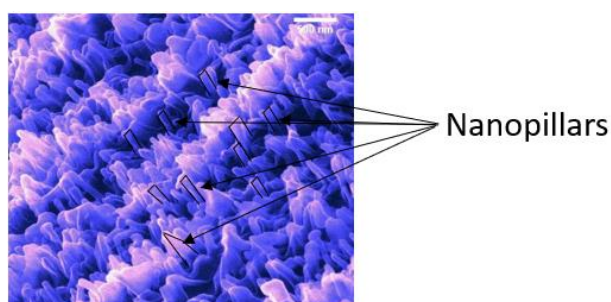
160   Figure 16: Pillar like nanostructure of the dragonfly wings. Reproduced with permission

161   from ACS Applied Materials and Interfaces 9, 6746 (2017) Copyright 2017, American

162   Chemical Society[15].

163

164   It has been proven that the bactericidal efficacy lies in the nanostructure both for the

165   dragonfly wings as well as cicada wings[68]. Despite this, a great advantage of dragonfly

166   wings over the cicada wings is its ability to kill both Gram-positive and Gram-negative

167   bacteria [45].

168   Bhadara *et al.*[69] were inspired by the dragonfly wings and attempted to mimic its

169   topography on titanium surfaces. Hydrothermal etching processes were employed, and *P.*

170   *aeruginosa* and *S. aureus* adhesion was tested. An increase in the CA and reduction in

171   the bacterial attachment was observed for both samples compared to the non-treated

172   titanium. Although the decrease in bacterial adhesion was observed for both cases,

173   significantly more non-viable *P. aeruginosa* were observed.

174   Modaresifar *et al*[70] gathered the currently available evidence to show how different

175   nanopatterned surfaces influence bacterial adhesion. The authors reviewed around 46

176   studies to conclude that the most common heights are between 100-1000 nm with a

177   diameter in the range of 10 to 300 nm and less than 500 nm spacings. They also concluded

178   that the most common structures that avoid bacterial adhesion were nanopillar-based

179   structures.

180   *2.2.5   Optical adjustment*

181   Optical adjustment is the ability of animals and plants to adapt and change their skin

182   colour according to the environment. The most well-known example is the chameleon

183   that appears to change its skin colour to increase survival chances[71]. These colour

184   changing properties lie in its skin cells called chromatophores[72]. These chromatophores

185   have a mixture of blue, white, red and yellow pigments, so with the correct combination

186   of pigments, the chameleon can adjust its skin to a wide range of colours depending on

187   the environment. The microstructure of chameleon skin consists of scales that can vary

188   in size between a few microns or millimetres (Figure 17a), which are covered by setae

189   ranging from 10 µm to 30 µm (Figure 17c)[73]. Several attempts have been made to

190   replicate the chameleon skin for different applications[74,75,76].

191

192

193
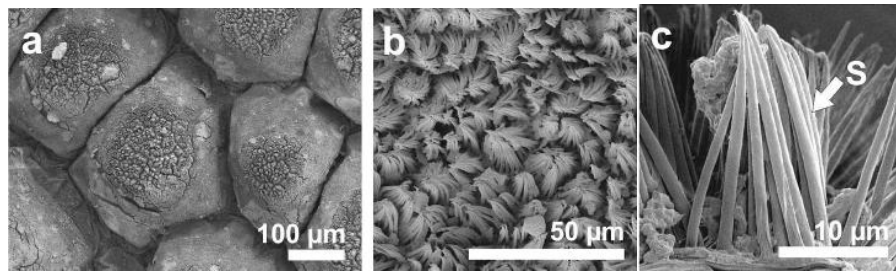
194 Figure 17: Scanning electron micrographs of the *Chameleo calyptratus.* a) Microstructure

195 of the chameleon skin with a scale-like microstructure. b) Setae covering the scale-like

196 microstructure. c) Cross-section of the scale with the setae (S). Reproduced with

197 permission from Sci. Report 4, 1 (2014) Copyright 2014, Springer Nature [73].

198 Moreover, some species of brittle stars (*Ophiocoma wendtii*) showed a colour changing

199 ability, from dark brown in the day to grey and black at night (Figure 18)[77,78]. This

200 reaction is due to dermal receptors that consist of single crystal-oriented calcite (10 µm-

201 15 µm)[31,78].

202
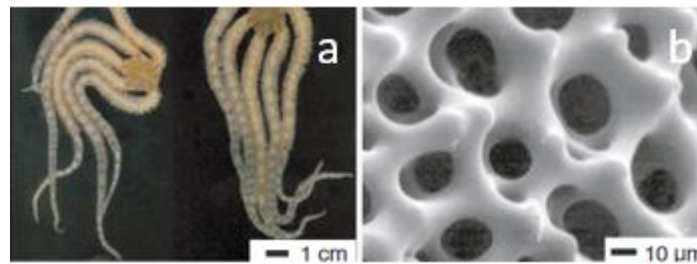
203 Figure 18 a) Brittle star image and b) SEM image of its microstructure. Reproduced with

204 permission from Nature 412 (2001) Copyright 2001, Springer Nature[78].

205

206 *2.2.6   Sensing to stimulus*

207 Some leaves such as of *Mimosa pudica* plants are extremely sensitive to physical contact,

208 they may open (Figure 19a) and close (Figure 19b) on being touched[79]. This extraordinary

209 property lies on its base where the pulvini are placed. The pulvini at the same time stores

210 the mechanical and photoreceptors that enable them to open and close[80]. Moreover, the

211 leaves of these plants can open in the night or day[81].

212
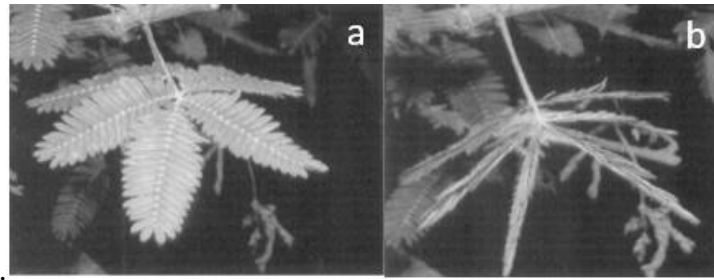
213 Figure 19: Leaves of the *Mimosa pudica* a) open and b) closed. Reproduced with
214 permission from J Bionic Engg. 4, 19 (2007) Copyright 2007, Springer[80].

215

216   *2.2.7   Hard and tough surfaces*

217 The main challenge for the human tooth is to be able to withstand constant loads and
218 stresses without fracturing. They are natural tissues with excellent mechanical properties
219 due to their hierarchical structures[82,83]. This hierarchical structure consists of an outer
220 layer called the enamel, an intermediate dentin layer and the pulp (the core), Figure 20[44].

221
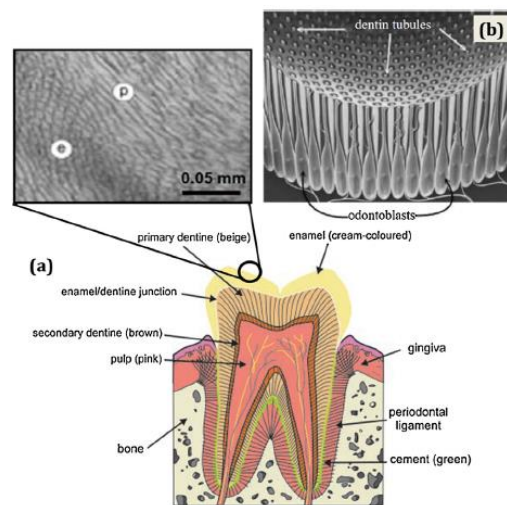
222 Figure 20 a) The main structure of human teeth, b) Tubular structure of dentin.
223 Reproduced with permission from CIRP J of Mfg. Tech., 62, 607 (2013) Copyright 2013,
224 Elsevier[31].

225 On one hand, the enamel is the hardest tissue type and is the one that offers continuous
226 mechanical and chemical resistance[84,85]. On the other hand, dentin consists of small
227 cylindrical tubes (1 µm to 3 µm diameter) surrounded by hydroxyapatite and organic
228 elements, dentin offers elasticity and mechanical strength to the teeth.

229   *2.2.8   Optics*

230   The colours of animals or plants are created by pigmentation, changing the angle of view

231   (iridescence), by architecture or a combination of the above. It is believed that those that

232   change colour as a result of architectural changes do so because of the interaction of light

233   and the hierarchical structures[86]. The *Morpho aega* butterfly wings apart from exhibiting

234   superhydrophobic properties, also exhibit blue iridescent colours (different colours if the

235   angle of view is changed)[87,88,89].

236   Another example of this is the peacock feather (Figure 21)[90]. The range of colours that

237   appear on its feathers is due to the 2D photonic crystal structure[91]. The microstructure

238   consists of 184 nm diameter and 3 µm to 14 µm length nanofibers, where the space

239   between the fibers are filled with air[92].

240
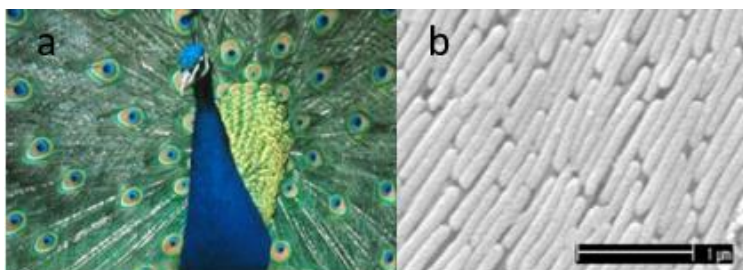
241   Figure 21: a) Peacock with its feathers. Reproduced with permission from Optics and

242   Laser Technology, 38, 329 (2006) Copyright 2006, Elsevier [90]. b) longitudinal cross

243   section of the barbs. Reproduced with permission from Prog Nat Acad Sci, 100, 12576

244   (2003), Copyright 2003, US National Academy of Sciences[91].

245

246   **2.3 Bactericidal CAD models inspired by nature**

247   Bacterial infection on surgical implants remains a formidable problem. Table II gathers

248   the reported dimensions of the most promising antibacterial and bactericidal surfaces (in

249   cases where the dimension was not explicitly reported, they were extracted using image

250   processing).

251   On the other hand, Table III shows a summary of some mimicked antibacterial surfaces

252   in terms of their dimensions and obtained outcomes.

253

Table II Natural dimensions of most promising antibacterial surfaces based on the literature.

Natural surface	Wettability (°)	Microstructure			Nanostructure			Reference
		Height (µm)	Base (µm)	Spacing (µm)	Height (nm)	Base (nm)	Spacing (nm)	
Lotus leaf	>150	-	Ø5-Ø9	-	-	Ø120	-	31
Lotus leaf	164	13	Ø10	-	780	Ø400	-	13
Lotus leaf	>150	10.4±0.8	8±2.4	19.5±12.5	530±150	Ø100±30	-	93
Shark skin	-	200-500	100-300	100-300		-		44
Shark skin	-	8	-	60		-		94
Gecko dorsal	151-155	50	Ø100-Ø190	50	Up to 4000	-	-	12
Gecko dorsal	-	-	160	210	3000	Ø350-Ø400	500	95
Cicada wing	144±7	Not hierarchical			200	Ø170	200	64
Cicada wing	-	Not hierarchical			300	Ø90	170	96
Cicada wing	146	Not hierarchical			146-157	Ø82-148	44-177	45
Cicada wing	159	Not hierarchical			200	Ø60 top and Ø100 base	170	63
Dragonfly wings	-	Not hierarchical			350	Ø80	150	96
Dragonfly wings	153	Not hierarchical			240	50-70	200	97

Dragonfly wings	-	Not hierarchical	Small: 189±67 Tall: 311±52	Small: 37±6 Tall: 57±8	-	[15]
Dragonfly wings	-	Not hierarchical	79.63-188.31	Ø83.25-Ø195.08	-	[98]

Table III Some bio-mimicked antibacterial surfaces and obtained outcomes.

Bio-inspiration	Fabrication process	Material	Surface type	Dimensions	Bactericidal effect	Reference
Dragonfly wing	Hydrothermal etching	Titanium	Nanowires	Ø40.2±20 nm	*P. aeruginosa:* 50% death. *S. aureus*: 20% death	[69]
Dragonfly wings	Reactive ion etching and CVD	Black silicon	Nanopillars	Ø20 nm-Ø80 nm Spacing: 200 nm- 1800 nm	Effective against Gram positive and Gram-negative bacteria.	[97]
Dragonfly wings	Ion etching	Silicon	Nanopillars	Ø220 nm and 4 µm height	83% of Gram negative (*E. coli*) and 86% of Gram positive (*S. aureus*) bacteria were killed	[99]
Cicada wing	Hydrothermal method	TiO$_2$	Nanowires	Ø100 nm and Ø10 µm-15 µm Heights: 3 µm	*P. aeruginosa*: More than 50% death *S. aureus*: Less than 5% death	[100]
Cicada wing	Glancing angle sputter deposition	TiO$_2$ on silicon substrate	Nanopillars	Ø33±7 nm Peak-peak: 158±105 nm	*E. coli*: 50% death *S. aureus*: Successfully colonized.	[101]

Cicada wing	Nanoimprinting lithography	PMMA	Nanopillars	Ø150 nm, 400 nm height and 150 nm spacing	-	102
Cicada wing	Thermal oxidation	Ti6Al4V	Nanospikes	Ø20 nm	Enhance the bactericidal activity against *E. coli*	103
Lotus leaf	Femtosecond laser	Titanium	Microbumps	Ø10 µm-Ø20 µm grains and 200 nm undulations	Lower adhesion of *P. aeruginosa* than polishes but increase of *S. aureus*.	46
Lotus leaf	Femtosecond laser	Titanium	Microbumps	Ø10 µm-Ø20 µm grains and 200 nm undulations	*S. aureus, S. epidermidis* and *P. maritimus* were able to attach to the surface.	104
Gecko skin	Template process	Epoxy resin	Nanoairs	2 µm-4 µm length 2 µm height 500 nm spacing and base	*S. mutans:* First 3 days lower adhesion than original skin. After 7 days more than natural skin *P. gingivalis*: Higher adhesion than natural skin.	62
Shark skin	Photolithography + ion etching	PDMSe	Grooves	2 µm width and spacing 3 µm height	Decrease of bacterial adhesion than smooth surface and avoid of biofilm formation.	55

Manufacturing of bactericidal surfaces requires good design and modelling of those structures to be developed. In this section, some bactericidal CAD models are proposed. More detailed information related to the dimensions of each structure is shown in Table IV.

As previously mentioned, the lotus leaf presents antibacterial properties due to its outstanding superhydrophobicity. Figure 22 depicts the lotus leaf surface structure and the proposed CAD model.
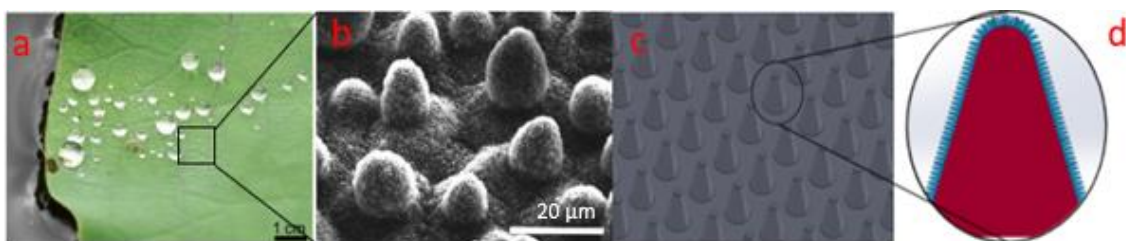
Figure 22: a) Natural lotus leaf. Reproduced with permission from Applied Materials and Interfaces, 9, 24381 (2017) Copyright 2017, ACS [93] b) Lotus leaf microstructure. Reproduced with permission from EPJ E, 16, 67 (2005), Copyright 2005, Springer [36] c) Lotus leaf microstructure model (Proposed CAD model corresponding to SEM image) d) lotus leaf micropapillae (red colour) with nanobranches (blue colour) (Proposed CAD model corresponding to SEM image). Scale bar is 20µm.

The nanostructure of cicada wings is bactericidal against Gram-negative bacteria. Figure 23 shows the model created to mimic cicada wings.
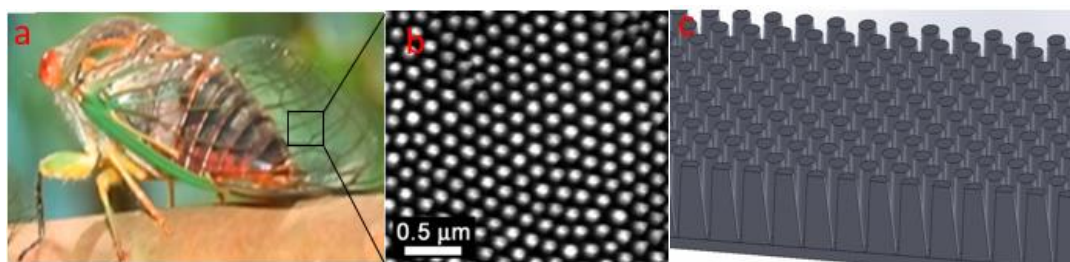
Figure 23: a) Cicada. Reproduced with permission from Trends in BioTechnology, 31, 295 (2013) Copyright 2013, Elsevier[38]. b) Cicada wing under SEM. Reproduced with permission from Int J of Nanomanufacturing, 5, 112 (2010) Copyright 2010, InderScience[96]. c) cicada wing nanostructure model (Proposed CAD model corresponding to SEM image).

Also, dragonfly wings possess excellent bactericidal efficacy against Gram-positive and Gram-negative bacteria. It is believed that this extraordinary property is due to the nanopillar based nanostructures. With this structure, nanopillars can damage the bacterial wall leading to its rupture. Figure 24 shows a model made for this nanostructure.
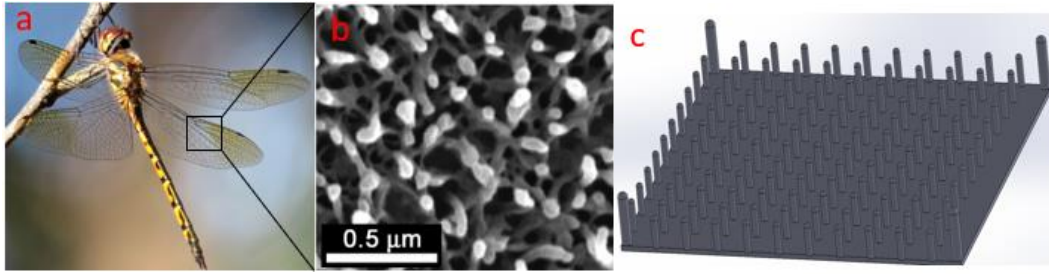
Figure 24) Dragonfly insect. Reproduced with permission from ACS Applied Materials and Interfaces 9, 6746 (2017) Copyright 2017, American Chemical Society[15] b) SEM image of a dragonfly wing. Reproduced with permission from Int J of Nanomanufacturing, 5, 112 (2010) Copyright 2010, InderScience[96] c) Dragonfly wing model (Proposed CAD model corresponding to SEM image).

The shark skin has been proven to be antibacterial due to its antibiofouling and self-cleaning properties[105]. It is documented that the most accurate reproduction of shark skin has been made by Sharklet AF[TM][55]. Figure 25 shows a representative model of Shark skin.
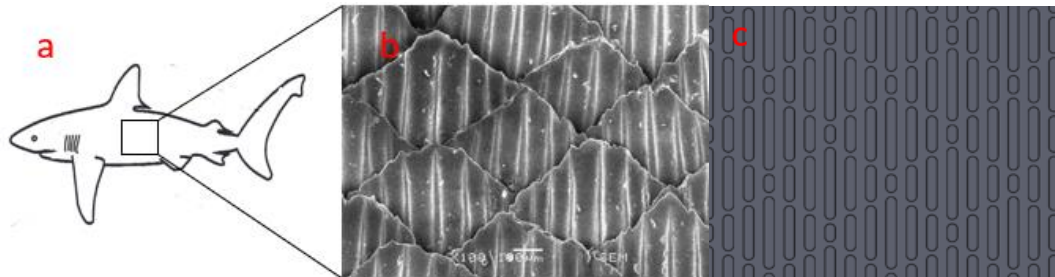
Figure 25 : a) Shark. Reproduced with permission from Exp Fluids 28 (2000) Copyright 2000, Springer [106] b) SEM of the shark skin microstructure. Reproduced with permission from J Mat Proc Tech, 212, 198 (2012) Copyright 2012, Elsevier [54] c) model of the shark skin based on the Sharklet AF[TM] (Proposed CAD model corresponding to SEM image).

This model consists of grooves with length varying from 4 µm to 16 µm, the height is 3 µm and the spacing between the grooves is 2 µm.

Moreover, Mann *et al.* [107] carried out a clinical study (simulation) where they used shark skin based micropatterned surfaces compared to an un-patterned surface. They observed a reduction of attached *S. aureus* but not complete abolition. Finally, Figure 26 shows the model for the Gecko animal skin.
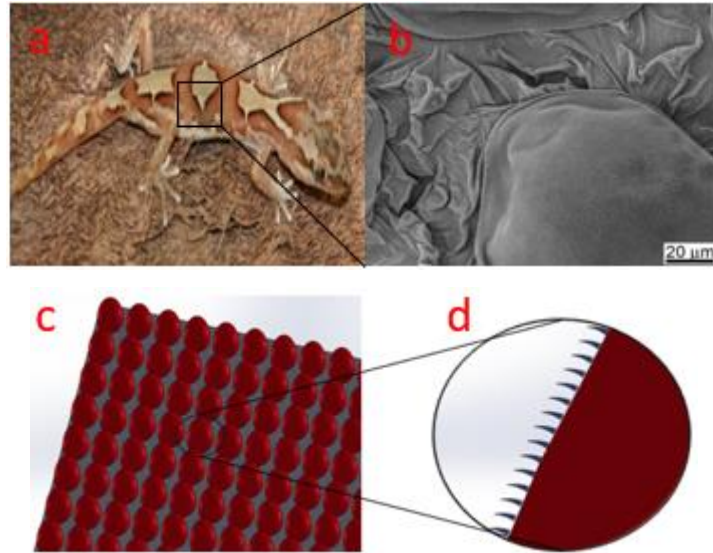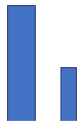
Figure 26 a) Gecko. B) SEM image of the dorsal dorsum of the gecko animal. Reproduced with permission from Acta BioMaterialia, 21, 109 (2015) Copyright 2015, Elsevier[12]. C) Scales at the micro level creating the first level of the hierarchical structures (proposed CAD model corresponding to SEM image). D) Cross-section view of the scales (red colour) and the nanohairs (blue colour) creating the second level of the hierarchical structure (proposed CAD model corresponding to SEM image).

The challenge of mimicking a natural surface lies both in the understanding of the multiscalar patterned hierarchical structures (see Table IV) as well as in the scalable fabrication of freeform surfaces. The next focus in Section 3 is to unravel the current understanding of the root causes of bactericidal properties and then Section 4 discusses the cutting-edge manufacturing methods to shed some light on the various possibilities and limitations of these methods.

Table IV Summary of the modelled bioinspired bactericidal structures dimensions

Natural surface	Microstructure			Nanostructure			Slope
	Height (µm)	Width (µm)	Spacing (µm)	Height (nm)	Width (nm)	Spacing (nm)	
Lotus leaf	10	Ø8	14	400	Ø200	150	
Cicada wing	Not hierarchical structures			200	Base: Ø100 Top: Ø60	110	
Dragonfly wing				Small: 189 Tall: 311	Small: Ø37 Tall: Ø57	Small. 170 Tall: 1943	
Shark skin	3	2x4-8-12-16	2	Not hierarchical structure			
Gecko skin	50	Ø150	170	700	Ø200	650	

1   **3. Bactericidal effect on surface properties**

2   Several attempts are made to model the bacteria-surface interactions and to understand

3   bacterial adhesion with a surface. In this section, some important surface properties

4   contributing to the observed bactericidal effect are presented and discussed. Figure 27

5   shows the representation of the bactericidal effect of surface properties.

6
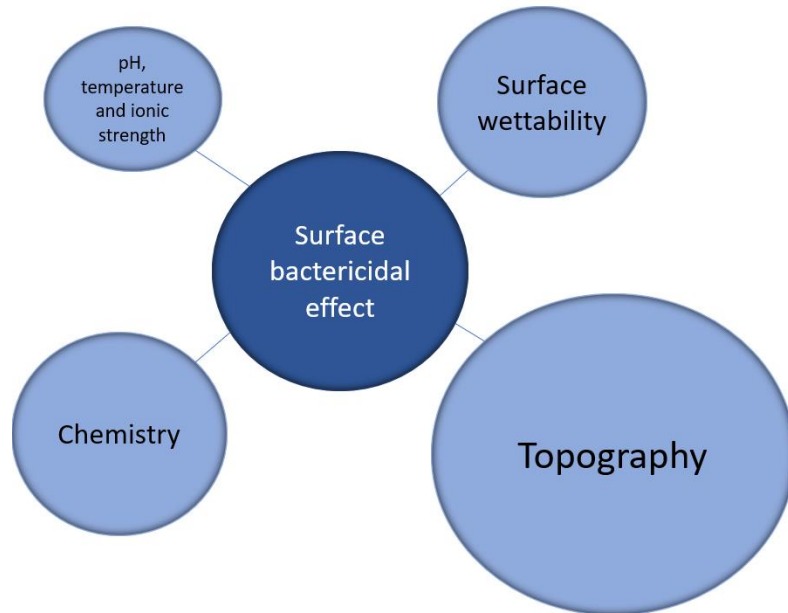
7   Figure 27: Illustration of the bactericidal effect and its root causes.

8   **3.1 Topography: Roughness and shape**

9   Several studies have tried to establish the relationship between surface roughness and

10   bacterial adhesion[108]. Truong *et al.*[109] performed a study where *S. aureus* and *P.*

11   *aeruginosa* were tested on titanium grade 2 samples with a surface treatment based on

12   equal channel angular pressing (ECAP). The surface roughness R_a (for an AFM measure

13   of 40 µm × 40 µm) of the samples were 2.90±1.74 µm and 3.80±1.39 µm for the

14   unprocessed and processed samples respectively. They concluded that the bacteria

15   preferentially adhered to the modified surface due to the increasing contact area at the

16   nanometer scale.

17   Ivanova *et al.*[110] studied the attraction and repulsion effect of *S. aureus* and *P. aeruginosa*

18   on different titanium thicknesses. It was observed that *S. aureus* were more adherent to

19   the same surface roughness than *P. aeruginosa*. They concluded that *P. aeruginosa*

20   attached on surfaces with an R_a value below 0.5 nm whereas *S. aureus* between 3 nm and

21   12 nm. It was also suggested that cell morphology could be one of the reasons why

22 bacteria exhibit different adhesion properties. Aykent *et al*[111] carried out experiments

23 where different materials with different surface finishes were tested against *S. mutans*. It

24 was observed that for the same materials, a decrease in the bacterial adhesion was

25 observed if the surface roughness decreases.

26 Moreover, Taylor *et al*.[112] studied the influence of the surface roughness on *S. aureus* and

27 *P. aeruginosa* bacterial adhesion. The R_a was varied from 0.04 µm to 7.89 µm, but despite

28 the difference in the surface roughness, similar bacterial adhesion was found both on

29 smooth and rough surfaces. They suggested that the bacterial adhesion was enhanced

30 when the features or dimensions are of the order of the bacterial size.

31 It can be observed that several works did not find any correlation between roughness and

32 bacterial adhesion. However, it should be noted that the current approaches of

33 characterizing surface roughness for the bactericidal effect typically rely on a single

34 amplitude two-dimensional parameter, R_a [110,112–114,115,116] which describes the arithmetical

35 average value of the deviation of the trace above and below the centre line. The limitations

36 of the use of the R_a parameter for surface characterisation has been previously

37 discussed[117]. Figure 28 shows an illustration of how completely different surface

38 roughness can provide the same R_a value. Thus, the analysis of roughness must involve

39 other parameters and not just the R_a to understand how the surface roughness behaves

40 against bacterial colonisation. One way around this would be to characterise a surface in

41 spatial frequencies.

42

Ra=3

Ra=3
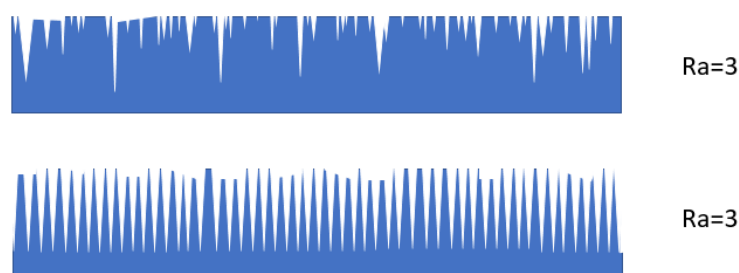
43 Figure 28: Same surface Ra with differing morphologies.

44 Even though surface roughness is an influential parameter for bacterial adhesion,

45 morphology is equally important[18]. The morphology can vary depending on the

46 manufacturing process, but some of the bactericidal examples can be grooves, pillars,

47 pits, or nanotubes.

48 This highlights the importance of introducing 3D area surface characterization processes

49 to provide a richer set of surface descriptors (including height, spatial, hybrid and

50 functional properties) since it is anticipated this could provide a correlation with

51 bactericidal effects, as previously suggested for other functionalities[118].

52 Ercan *et al.*[119] manufactured Ti nanotubes with different diameters varying from 20 nm

53 to 80 nm. It was observed that the increase in the diameter decreases bacterial adhesion.

54 Conversely, in the study carried out by Yu *et al.*[120]where they manufactured Ti nanotubes

55 from 30 nm to 120 nm, the increase of the diameters increased the bacterial adhesion.

56 Bandara *et al.*[15] tested *E. coli* bacteria and reported the interaction of the bacteria and the

57 surface using a Transmission Electron Microscope (TEM) measuring system. A model

58 was suggested to explain why bacteria rupture due to the nanopillar based structures.

59 Their proposed mechanism is shown in Figure 29.

60
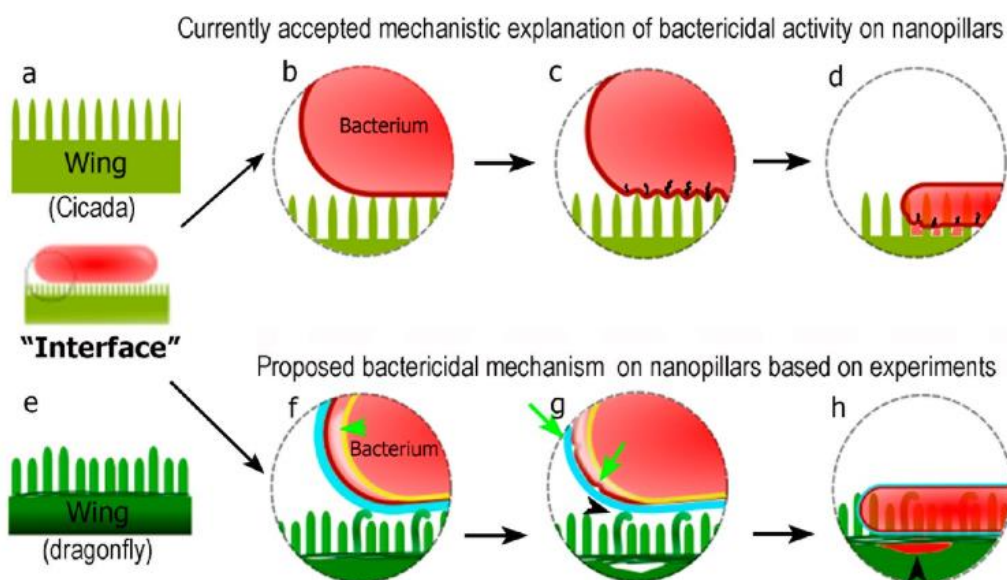
61 Figure 29: Representation of the bactericidal mechanisms of the nanopillars. a)-d)
62 currently accepted mechanism between the interaction of bacteria-nanopillars. e)-h)
63 proposed mechanism a) Cicada wing nanostructure with tall pillar at the same height. b)
64 bacterium approaching the nanostructure. c) bacterial membrane starts rupturing between
65 the pillar like structures due to stretching. d) The bacteria get ruptured and the cytoplasm
66 starts leaking leading to bacterial death. e) Dragonfly wing illustration with variable
67 lengths of pillars. f) The approaching bacterium bends the taller pillars, but it does not
68 puncture the membrane. g) After adhesive forces are applied to the bacterial surface, the
69 two membranes (EPS in the blue and outer membrane in red) start separating. h) Finally,
70 the cytosol of the bacterium leaks, leading to cell death. Reproduced with permission
71 from ACS Applied Materials and Interfaces 9, 6746 (2017) Copyright 2017, American
72 Chemical Society[15].
73

74 In another study carried out by Hochbaum et al.[121], the spacing between pillars and the

75 antibacterial effect was analysed. Also, Lorenzetti et al.[122] studied the influence of the

76 spacing of the grooves. Related to the dimensions of the features, Anselme et al.[123] made

77 a concise review of the interaction between the nanostructuring of the surface and its

78 effect on bacterial adhesion.

79 Wu et al[124] fabricated pillar like structures made by nano-replication technology in the

80 polymeric material. Different models (with different sizes, heights and spacings) were

81 prepared and tested. They concluded that the density of the pillars had a critical impact

82 on the bactericidal efficacy of the surface. Moreover, from this study it may be observed

83 that the best model has a similarity with the dragonfly wings. Apart from this study, a

84 biophysical model of the bacterial stretching was developed where the stretching degree

85 and the pillar density were evaluated.

86 Li et al[125] created a thermodynamic model that predicted the nanopillar radius that

87 ruptures the bacterial wall. It should be noted that this model was only valid for Gram-

88 negative bacteria due to their thinner bacterial wall.

89 Moreover, Cunha et al.[126] and Chan et al.[127] created structured surfaces by laser ablation

90 on titanium samples. They both concluded that the enhancement of bacterial suppression

91 was due to the similar dimensions between the bacterial diameter and the surface. This

92 theory was also supported by other authors [18,117,128–130] due to the smaller contact area

93 between the bacteria and the surface.

3.2 Wettability

95 The fundamental models of wettability of surfaces were discussed in the earlier section.

96 Based on these known theories, several studies have attempted to clarify the effect of the

97 wettability on bacterial adhesion [14,117,128,131,132]. Tang et al. [131] fabricated

98 superhydrophobic surfaces on titanium samples and they concluded that the

99 superhydrophobic surfaces may inhibit S. aureus adhesion, with hydrophilic surfaces

100 attracting S. aureus. Similar conclusions were drawn by Tripathy et al.[10], Lee et al or

101 Fadeeva et al.[46]. Moreover, it has been reported that hydrophobic surfaces are able to

102 reduce the adhesion of S. aureus[133]. Conversely, some studies concluded that bacterial

103 repulsion was enhanced by hydrophilic surfaces[126,131]. Thus, the extant literature does not

104 clarify which type of surface repels S. aureus bacterial adhesion; superhydrophobic

105 surfaces or hydrophilic surfaces.

106   **3.3 Chemistry**

107   The chemical composition of the surface can also alter bacterial adhesion. Campoccia *et*

108   *al.*[134] proved that the chemical composition of the surface may alter bacterial adhesion.

109   Researchers concluded that the crystalline structure of titanium oxide (the anatase phase)

110   possess more bactericidal activity than the amorphous phase[127,135]. The same conclusions

111   were found by Del Curto *et al* [136] and Giordano *et al.*[137]. Chu and Williams[138] investigated

112   the effect of the chemical composition of *S. aureus* and *E. coli* for respond to different

113   materials. Ivanova *et al.*[97] fabricated black silicon samples inspired by dragonfly wings

114   by ion-beam etching and compared the bacterial adhesion to natural dragonfly wings.

115   They concluded that the number of attached bacteria to the dragonfly like textured black

116   silicon was similar to those attached to the real dragonfly wing. This suggests that

117   chemical composition has a minor effect compared to the surface topography. However,

118   the effect that the removal of wax can play is known and was discussed earlier (section

119   2.2.1) and this counteracts this conclusion.

120   *3.3.1   Bactericidal activity of silver and copper*

121   Over the last few years, special attention has been focused on introducing metallic

122   nanoparticles such as Ag, Cu, Zn, or Au onto metallic or polymeric materials due to their

123   high bactericidal activity[139].

124   Silver is one of the most well-known natural bactericidal agents due to its high toxicity

125   to most of the micro-organisms[140]. It is believed that the bactericidal effect of silver relies

126   on the interaction between silver ions and thiol groups of vital enzymes that passivates

127   them. Several studies have been made on the interaction and use of Ag^+ ions to repel or

128   kill bacterial strains[141,142,143]. These studies concluded that silver nanoparticles can repel

129   the bacteria attachment by the rupture of their membranes.

130   Moreover, copper nanoparticles are also well-known for their bactericidal activity

131   employed for sterilizing liquids, textiles or human tissues for over a few decades [144]. The

132   current challenge relies on the synthesis of Cu nanoparticles because they undergo rapid

133   oxidation into Cu^{2+} ions in air and in aqueous media [145]. Table V presents a

134   comprehensive summary of the various types of particle used, doses employed and

135   bactericidal response, as well as the manufacturing process employed to date in this

136   regard.

Table V Bactericidal efficacy of different nanoparticles

Nanoparticle	Dosses	Bacterial response	Manufacturing process	References
3 sizes of Ag	0.01 M	*S. mutans* reduction. Bactericidal response depends on the size.	Gallic acid in an aqueous chemical reduction method	[146]
Ag	4.26% using EDS	Remarkable antibacterial effect against *S. aureus* and *E. coli*	Silanization method	[147]
Ti nanotubes + Ag	0.5 M, 1 M, 1.5 M and 2 M	Significant reduction of the osteoblast cells.	Immersion in a silver nitrate solution	[148]
Ag+ + hydroxyapatite	296 mg/ml	More than 99% of *S. aureus* and *E. coli* were killed after 24 h	Dipping	[149]
Ag	25-100 mg/l	Concluded a 3 step process of P. Aeruginosa bacterial wall rupturing	-	[141]
Ag and ZnO	10 mM	Small reduction of *B. subtilis* bacteria reproduction	-	[150]

3.3.2 *Bactericidal activity of metal oxide nanoparticles*

Despite silver being one of the most well-known bactericidal materials, many other nanoparticles are also known to cause bactericidal activity. Over the last few years, several metal oxide nanoparticles such as aluminium oxide (Al_2O_3), calcium oxide (CaO), magnesium oxide (MgO) or copper oxide (CuO) have attracted scientists to explore their antibacterial efficacy[151]. Moreover, the mechanism that explains the interaction between nanoparticles and bacteria is also reported by Slavin et al. [152] while they advocated the use of nanoparticles to rupture bacteria, they also highlighted that the antibacterial nanoparticles in high concentrations can be toxic and unhealthy.

Dizaj et al.[153] mentioned that the morphology of the nanoparticle has a big impact on the bactericidal effect: the surface/volume ratio of the nanoparticle. It was deduced that a smaller nanoparticle exhibits higher bactericidal effect.

Based on the reviewed literature[151,152,153,154] the main mechanisms of the bacterial metals, their characteristics and potential applications have been gathered in Table VI. Also, the antimicrobial effects of most used metal oxide nanoparticles are gathered in Table VII.

Table VI: Antibacterial mechanism for antibacterial metals, their characteristics, and potential applications

Antibacterial mechanism	Corresponding antibacterial material	Characteristics	Prospective applications
Slow release metal ion sterilisation	Copper, silver, metal ion phosphate antibacterial materials, etc.	High chemical activity provides long term and efficient slow release antibacterial materia	Widely used in medical applications, stainless steel, water treatment. Prevent bask in liquid coatings and fabrics. But these materials tarnish easily and are expansive, which limits their applications
Slow release metal ion sterilisation and photocatalytic sterilisation	Hydroxyapatite, Ag-carrying phosphate antibacterial materials, etc.	Phosphoric acid double salt has a strong adsorption function, large specific surface area, nontoxic, stable chemical properties; good combination of efficiency and lasting slowrelease performance	
Slow release metal ion sterilization, photo-catalytic sterilization and reactive oxygen species antibacterial mechanism	ZnO materials, TiO2 materials	Stable chemical properties, under UV irradiation show broad spectrum antimicrobial properties, good pH stability, nontoxic, abundant raw material sources, low cost.	Used in fiber, plastic, ceramic, coating, biomedical and other fields

Table VII: Antimicrobial activity of metal oxide nanoparticles

Metal oxide NPs	Test organism	Antimicrobial action
Aluminium oxide (Al$_2$O$_3$) NPs	*Escherichia coli*	Growth inhibition of *Escherichia coli*
Antimony trioxide (Sb$_2$O$_3$) NPs	*Escherichia coli, Bacillus subtilis* and *Staphylococcus aureus*	Toxic to all the three microbes
Bismuth oxide (Bi$_2$O$_3$) NPs	*Pseudomonas aeruginosa, Acinetobacter baumannii* and *Escherichia coli*	No effect against all tested microbes
Calcium oxide (CaO) NPs	*Lactobacillus plantarum*	Higher bactericidal activity
Cerium oxide (CeO) NPs	*Escherichia coli, Shewanella oneidensis* and *Bacillus subtilis*	No effect on *Shewanella oneidensis*
Cobalt oxide (Co$_3$O$_4$) NPs	*Staphylococcus aureus* and *Escherichia coli*	Showed antimicrobial activity on tested bacteria
Copper oxide (CuO) NPs	MRSA, *Staphylococcus epidermis*, *Pseudomonas aeruginosa*, *Proteus* sp. *Staphylococcus aureus*, *Bacillus subtilis*, *Escherichia coli*; fish pathogens: *Aeromonas hydrophila*, *Pseudomonas fluorescens*, *Flavobacterium* sp. and *Branchiophilum* sp	Active against all the tested microbes
Magnetite (Fe$_3$O$_4$) NPs	*Escherichia coli*	Concentration-dependent bacteriostatic action
Iron oxide (FeO) NPs	*Staphylococcus aureus, Shigella flexneri, Escherichia coli, Bacillus licheniformis, Bacillus subtilis, Brevibacillus*	Moderate antibacterial activity against 6 Gram-positive and 2 Gram-negative bacteria

	brevis, *Vibrio cholerae*, *Pseudomonas aeruginosa*, *Staphylococcus aureus* and *Staphylococcus epidermis*	
Magnesium oxide (MgO) nanowires	*Escherichia coli* and *Bacillus* spp.	Lower bacteriostatic activity
Titanium dioxide (TiO₂) NPs	MRSA	Exhibited antimicrobial effect on tested isolates
Zinc oxide (ZnO) NPs	MSSA, MRSA and MRSE, *Streptococcus agalactiae*, *Staphylococcus aureus*, *Escherichia coli*, *Bacillus subtilis*, *Salmonella paratyphi*, *Staphylococcus aureus*, *Pseudomonas aeruginosa*, *Mycobacterium smegmatis*, *Mycobacterium bovis*, *Klebsiella pneumoniae*, *Enterobacter aerogenes*, *Candida albicans*, *Malassezia pachydermatis*, *Bacillus megaterium*, *Bacillus pumilus* and *Bacillus cereus*	Active on tested microbes
Zinc/iron oxide composite NPs	*Escherichia coli* and *Staphylococcus aureus*	Exhibited greater antibacterial activity with higher Zn/Fe weight ratio
ZnO-loaded PA6 nanocomposite	*Staphylococcus aureus* and *Klebsiella pneumoniae*	Dose-dependent antibacterial action
Nanosilver-decorated TiO₂ nanofibres	*Staphylococcus aureus* and *Escherichia coli*	Increased antimicrobial effect
Hybrid CH-α-Fe₂O₃ nanocomposite	*Staphylococcus aureus* and *Escherichia coli*	Improved antibacterial activity
Zinc-doped CuO nanocomposite	*Escherichia coli*, *Staphylococcus aureus* and MRSA	Remarkable biocidal activity

42

PEI-capped ZnO NPs	*Escherichia coli*	Exhibited better antibacterial activity
Chitosan-based ZnO NPs	*Candida albicans*, *Micrococcus luteus* and *Staphylococcus aureus*	Showed biofilm inhibition against *Micrococcus luteus* and *Staphylococcus aureus*
Carvone functionalized iron oxide	*Staphylococcus aureus* and *Escherichia coli*	Inhibited colonization and biofilm formation
Silver-decorated titanium dioxide (TiO$_2$: Ag) NPs	MRSA and *Candida* sp.	Conferred antimicrobial effect on tested microbes
Graphene oxide modified ZnO NPs	*Escherichia coli*, *Bacillus subtilis*, *Salmonella typhimurium* and *Escherichia faecalis*	Excellent antibacterial activity
NPs: nanoparticles; MRSA: methicillin-resistant *Staphylococcus aureus***; MRSE: methicillin-resistant** *Staphylococcus epidermidis***; MSSA: methicillin-sensitive** *Staphylococcus aureus***; PEI: polyethyleneimine.**		

3.3.3 Bactericidal surface treatments obtained by silver ion implantation

Ion implantation, unlike a surface coating, allows an atomic species (in an ionized form) to penetrate onto the surface (sub-surface) which offsets the risk of delamination that is one problem with the coatings reported in the literature. Similar to other surface manufacturing processes, ion implantation improves the corrosion resistance, wear resistance, hardness, bioactivity and antibacterial effect of biomaterials compared to their pristine forms. Since it is a surface modification technique, the favourable bulk properties of the substrates are preserved. In addition, one of the most valuable advantages of this low-temperature surface treatment technique is that it can strictly control the concentration and depth distribution of implanted ions by adjusting the processing parameters.

Among different ion implantation techniques, Plasma-Immersion Ion Implantation (PIII) is a suitable, versatile and promising method for the surface modification of complex-shape materials without the line-of-sight limitations of conventional ion implantation techniques. Generally, a PIII system comprises of a vacuum chamber with a workpiece stage, a plasma source and a high-voltage pulse modulator. During PIII processing, samples are immersed in a high-density plasma and biased to a high negative pulsed potential relative to the vacuum chamber wall, which repels electrons away from the samples, while driving the positive ions of the plasma towards them, creating a plasma sheath around the samples. Therefore, ions become implanted into the sub-surface, creating a thin sublayer in the range of a few tens of nanometers. In addition, consecutive etching, ion implantation and deposition processes are possible by varying the processing parameters.

PIII technology offers unique advantages for treating various biomaterial surfaces. Previous shortcomings of poor coating adhesion (easy delamination) or roughness modification have been overcome by using PIII. Furthermore, PIII can be combined with different plasma ion sources: cathodic arc, metal vapor vacuum arc (MEVVA), electron cyclotron resonance (ECR), Kaufman, etc.

One of the promising applications of this technique is the possibility of creating antibacterial surfaces by the implantation of biocidal elements such as Ag, Cu, or Zn, or its combination with bioactive elements such as Ca and Mg.

Table VIII summarizes the main processing parameters (ion type, substrate, ion source, bias/acceleration voltage and ion dose) and the bactericidal effect results obtained by

silver ion implantation (and its combination with other elements) conducted by different research groups.

It can be observed that most of these works have demonstrated a bactericidal efficacy against *E. coli* and *S. aureus*. However, it has also been shown that silver ion implantation treatments are effective against a number of pathogens found in infectious processes such as peri-implantitis: *P. gingivalis*, *A. actinomycetemcomintas*, *P. aeruginosa*, *C. albicans*, *S. mutans*, *A. actinomycetum*, *F. nucleatum*, *B. forsythus*, among others[155,156,157,158,159]

It should be noted here that some of these studies report that the silver ions implanted in the surface agglomerate in the form of nanoparticles. Despite the potential toxicity of nanoparticles, an *in vivo* study carried out by H. Qin *et al* [155] on Labrador dogs demonstrated that the treatment is not only biocompatible but also favors osseointegration, arguing that the plasma immersion ion implantation technique reduces the mobility of the nanoparticles and promotes, in turn, cytocompatibility.

Similarly, an *in vivo* study on Sprague Dawley rats conducted by Mei *et al* [156] established the optimal bias voltage for obtaining a bactericidal effect without causing any inflammatory phenomena due to the possible toxicity of silver.

Another *in vivo* study on Sprague Dawley rats demonstrated the synergistic bactericidal and osteogenic effect provided by silver and zinc nanoparticles obtained by the simultaneous ion implantation of both elements using cathodic arc sources[160].

More recently, Cao *et al*. demonstrated the osteogenic effect of bone marrow stem cells induced by silver ion implantation on implants inserted in rats[161].

Table VIII: State of the art of bactericidal treatments based on silver ion implantation:

Ion	Substrate	Plasma ion source	Bias/Acceleration voltage (kV)	Dose ions/cm^2	Bacteria tested _In vivo_ studies	Reference
Ag	Ti	ECR	2	$1.5 \cdot 10^{16}$	S. aureus	[162]
Ag	Ti	Cathodic arc	30	-	_E. coli, S. aureus_	[163]
Ag	Ti	Cathodic arc	20	-	_In vivo_ positive response	[161]
Ag	Ti	MEVVA	40	10^{16}	_S. aureus_	[164]
Ag	Ti	Cathodic arc	15	-	_F. nucleatum, S. aureus_	[159]
Ag	TiO$_2$-Ti	MEVVA	70	$10^{17} - 2 \cdot 10^{18}$	_S. aureus_	[165]
Ag	316LVM	Cathodic arc	30	-	_E. coli, P. aeruginosa, S. aureus, S. epidermis_	[155]
Ag	TiO$_2$	MEVVA	40	$(0,5-10) \cdot 10^{16}$	_E. coli_	[166]
Ag	Ti	Cathodic arc	30	-	_In vivo_ positive response Osseoconductive treatment	[167]

Ag	TiO$_2$-Ti	Cathodic arc	0,5-1	-	*P. gingivalis, A. actinomycetemcomitans.* *In vivo* positive response	[156]
Ag	CrN-316L	Kaufman ion source	100	$5 \cdot 10^{16}$-10^{17}	*E. coli, S. aureus*	[168]
Ag	TiO$_2$-Ti	MEVVA	65	$(1\text{-}20) \cdot 10^{17}$	*S. aureus*	[169]
Ag	AISI 420	MEVVA	50	10^{17}	*E. coli*	[170]
Ag	Ti	Cathodic arc	15	-	*S. mutans. P. gingivalis, C. albicans*	[157]
Ag	Ti	----	15	10^{16}	*A. actinomycetum, F. nucleatum, C. rectus, P. micros, B. forsythus*	[158]
Ag	Ti	Cathodic arc	30	-	*E. coli, S. aureus*	[171]
Ag	317L, TiN-317L	MEVVA	70	$5 \cdot 10^{16}$ – $5 \cdot 10^{18}$	*S. aureus*	[172]
Ag	Pyrolytic carbon	MEVVA	70	$5 \cdot 10^{14}$-$5 \cdot 10^{18}$	*E. coli, S. aureus*	[173]
Ag/Zn, Ag+Zn	Ti	Cathodic arc	30	-	*E. coli, S. aureus.* *In vivo* positive response	[174]

Ag, Ag+Mg	Ti	Cathodic arc	30-40	-	*E. coli*	[175]
Ag/Ca, Ag+Ca	Ti alloy	MEVVA	50	10^{17}	*E. coli, S. aureus*	[176]
Ag/Zn, Ag+Zn	Ti	Cathodic arc	30	-	*E. coli, S. aureus* *In vivo* positive response	[160]
Ag+Cu	AISI 420	MEVVA	50	$2 \cdot 10^{17}$	*S. aureus, A. niger*	[177]
Ag/Cu	Ti6Al4V	CHORDIS	2-20	10^{15}-10^{17}	*E. coli, S. aureus*	[178]
Ag/Cu	Polyethylene	Cathodic arc	5	-	*E. coli*	[179]
Ag/Cu	317L, Ti, TiAlNb	MEVVA	80	10^{17}	*S. aureus*	[180]

3.3.4   *Bactericidal carbon-based coatings doped with silver*

In the last two decades, amorphous diamond-like carbon (DLC) coatings have received great interest due to their exceptional properties such as high hardness, low friction, chemical inertness, corrosion protection, biocompatibility, optical transparency in the IR spectral range and tunable electrical resistivity[181,182]. Nowadays, DLC coatings have been industrially implemented in many engineering applications where excellent tribological properties are required. Additionally, the outstanding biocompatibility of these coatings offers a wide range of potential biomedical applications for the improvement of the mechanical, chemical and biological response of prostheses and implants[183]. Specifically, the possibility of doping DLC coatings with bactericidal elements such as silver has resulted in intensive research in this field.

The main bactericidal effect of silver is conducted through the release of Ag^+ ions via an oxidative reaction in an aqueous solution or a biological medium[184]. The kinetics of this dissolution process relates to the duration of the antibacterial effect, can increase exponentially if silver is used as nanoparticles due to its higher surface to volume ratio. Furthermore, the stability and the long-term antibacterial effect of Ag-doped DLC depends on various factors such as surface energy, mean roughness, micro- and nanostructure of the coating, as well as the concentration and distribution of silver across the thickness of the coating (dispersed or agglomerated in the form of nanoparticles).

Various methods have been reported of preparing Ag-DLC coatings with different silver concentrations specifically for biomedical applications which include RF or DC reactive magnetron sputtering of the silver target in a hydrocarbon atmosphere[185,186,187,188,189,190,191,192,193], DC magnetron sputtering of silver and graphite targets[194,195,196], hybrid RF/magnetron sputtering plasma assisted chemical vapor deposition (RF/MS PACVD) [197,198], dip coating of a PVP polymer film with a colloidal dispersion of stabilized silver nanoparticles transformed to DLC by ion implantation [199,200,201], polyethylene transformed to DLC by silver implantation[202,203], thermionic vacuum arc[204], silver nanoparticle solution combined with a DLC coating obtained by PACVD[205], cathodic arc deposition[206,207,208,209,210] and pulsed laser deposition[211,212,213,214,215]. Most of these works demonstrate good antibacterial efficacy of these coatings against *E. coli*, *S. aureus* and *S. epidermidis* for silver concentrations higher than about 2 at.%. Also, Ag-doped DLC coatings offer an antibacterial activity over a wide spectrum of other bacterial species: *C. jejuni* and *L. monocytogenes*[192]; *A. israelii*,

S. sanguinis, F. nucleatum, C. rectus, *E. corrodens*, *P. micra*, *P. intermedia*, *A. actinomycetemcomitans* and *P. gingivalis*[196]; *S. warneri*[212], and *P. aeruginosa*, *E. faecalis* and *C. albicans*[215]. On the other hand, good hemocompatibility of DLC coatings with a silver concentration of 9.7%[185], and between 70-90%[209] has been demonstrated. Furthermore, Chekan *et al.*[210] have shown that DLC coatings doped with a silver concentration of 3.5% to 6.5% possess an inhibiting effect on the growth of some tumor cells.

Despite good antibacterial efficacy shown by Ag-doped DLC coatings, the main concern related to its applicability in prostheses and implants lies in the adjustment of the optimal concentration of silver to obtain a significant antibacterial activity by suppressing cytotoxicity. In this sense, coatings with a silver concentration as low as 1.6 and 2.1% have shown significant levels of cytotoxicity[191]. Other studies point to a silver concentration thresholds of 4.5%[201] or 5.4%[197], above which the coating becomes cytotoxic. In this regard, excellent non-cytotoxic properties have been reported for DLC coatings with silver concentrations of 2.0%[198] and 3.1%[193]. On the contrary, non-cytotoxic coatings have been obtained for silver concentrations of 5.6%[206] and 6%[196]. More detailed studies demonstrate that the adequate concentration of silver, in terms of physical-chemical properties, for providing an efficient protection against microbial colonization and a non-cytotoxic behavior, ranges between 2% and 7%[213] and more accurately 3.6%[215].

The disparity of these results reveals that the antibacterial activity and cytotoxicity of these types of coating not only depends on the concentration of silver, but, as mentioned above, other factors determine the kinetics of the release of Ag^+ ions. However, given the published results, a conservative value of the concentration of silver that guarantees an antibacterial effect without causing cytotoxicity would be around 2%.

3.4 pH, ionic strength and temperature

In most of the studies, a lot of importance has been attributed to the surface wetting, chemical composition, or morphology. However, since bacterial adhesion is governed not only by one surface property, a small change in the pH of the environment, ionic strength, or temperature around the implant may also alter bacterial adhesion. For example, the effect of the ionic strength was explored by Morisaki *et al.*[216] Also, Hamadi *et el.*[217] studied the effect of the pH on bacterial adhesion and they concluded that less bacterial adhesion was observed on the extreme values (2 and 12) whereas, at a pH of 5, most

bacteria flourish. Garret et al.[218] presented a very comprehensive review illustrating the effect of the pH and temperature on the bacterial colonisation.

4. Ultra-precision manufacturing of biomimetic surfaces

In this section, various nano and micro-manufacturing methods applied to date for producing patterned biomimetic surfaces are reviewed to highlight and discuss the limitations and advantages of each technology.

According to Bruzzone et al.[219] and Jaggessar et al[45], various surface modifications can be divided into three streams as additive methods, subtractive methods, or re-structuring (patterning – theoretically involving no loss or addition of material onto the surface). Moreover, according to Mijatovic et al [220] and Biswas et al [221], the additive method is referred to being a bottom-up method and the subtractive method is referred to as a top-down method.

Figure 30 shows an overview of the classification of the different manufacturing techniques employed to modify the surfaces.

Additive methods
- Chemical routes
- Physical routes

Subtractive methods
- Beam based routes
- Mechanical routes
- Chemical etching

Surface patterning methods
- Chemical routes
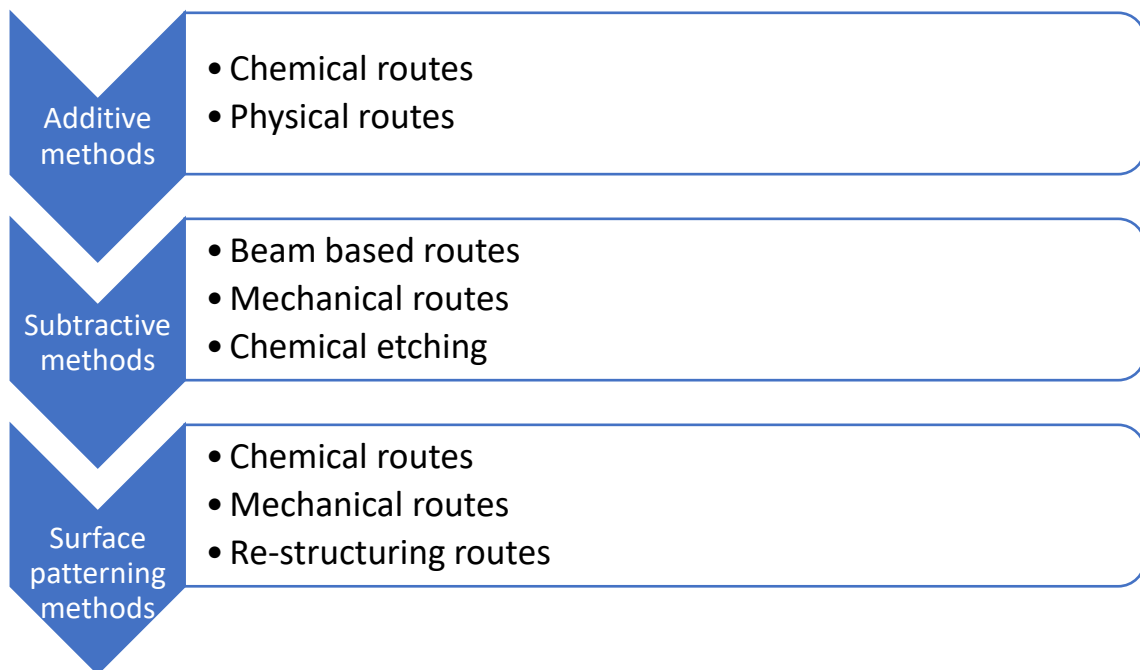- Mechanical routes
- Re-structuring routes

Figure 30: Overview of the manufacturing techniques classification.

4.1 Additive processes

Additive methods rely on adding the material to the desired surface. Most of those methods are related to the deposition of coatings or implantations. Table IX summarizes various additive methods reviewed by Bruzzone et al.[219].

Table IX Classification of additive type surface modification techniques

Additive processing		
Chemical processes	Chemical conversion coating	Patterned chromating
		Patterned phosphating
	Chemical deposition coatings	Chemical vapour deposition (CVD)
		Patterned autocatalytic plating
		Anodising
		*Electro-deposition
		Sol-gel
	Patterned precipitation coating	
Physical deposition	Inkjet	
	Patterned curing	
	Physical vapour deposition (PVD)	
	Painting	
	*Deposition of micro- or nanoparticles	
	*Self-assembling in polycrystalline films	
	Vacuum casting	

*Considered as an Ultra Precision manufacturing technique.

The chemical processes shown in Table IX involves printing the surface with inks that can inhibit or promote some chemical or electrochemical reactions, so some patterned coatings can be achieved [219]. These for instance include Roll-to-Roll (R2R) manufacturing routes which have started to become an ultra-precision fabrication technology [222]. In the past, anodising processes have been used[137,223,224,225] to inhibit bacterial colonization. Driven by an electrolysis approach, this process consists of chemical reactions between a cathode and an anode leading to thin film formation on the surface[8]. Also, chemical vapour deposition (CVD) has been employed [226,227,228] with different particles in order to avoid bacterial adhesion on different surfaces as well as physical vapour deposition[229]. CVD is a chemical reaction-based method that is used to fabricate advanced functional surfaces. Different types of CVD methods can be used such

as plasma-enhanced CVD, catalyst assisted CVD or initiated CVD. The major limitation of this method of harnessing advanced and complex surface functionalities lies in the difficulty in controlling the precision of the surface detail[37]. Park *et al* [230] fabricated a multifunctional surface based on nanotaper structures (based on pitcher plants) which gave them antifogging and superhydrophobic abilities.

The deposition of micro- or nanoparticles has also been used to reduce bacterial adhesion. Ion implantation is another technique used in this area[9,231]. The particles are implanted between 0.1 µm and 1 µm depth[232]. It has been reported that Ag, Cu, Zn-Ag, Ca ions have been used for *S. aureus* suppression[174,176,178,180,233,234]. Table X summarizes the additive fabrication techniques used to create bactericidal surfaces.

Table X Additive manufacturing processes employed to suppress the bacterial adhesion

Additive process	Materials employed	Bacterial response	Reference
Anodization	Grade 2 Ti and Ti6Al4V	Successful bactericidal activity of the anodized samples	137
Nanoimprint lithography	PMMA	50% decrease of *E. coli* bacteria compared to polished ones	235
Electrodeposition	Au nanoparticles	All structures Au nanoparticles exhibit great bactericidal activity against *S. aureus*	236
Physical vapour deposition	Titanium coated with copolymers	Decrease of the *S. aureus* bacteria.	237
Spraying deposition	Titanium anodized substrate coated with polylactide.	0.5% of PLA concentration showed the best inhibition rate to *S. aureus*.	238
Lyophilization method	Titanium nanotubes loaded with gentamicin	Reduction of *S. aureus* and enhance osteoblast activity	239

Physical vapour deposition	Grade 2 Ti with silver coating	Reduce the bacterial adhesion of *S. epidermidis* and *K. pneumoniae*.	[229]
Chemical vapour deposition	Silicone elastomer	Decrease of *S. aureus* bacteria compared with uncoated sample	[240]
Ag and Cu Ion implantation	317L, Pure Ti, TiAlNb	Improved the antibacterial properties of the substrates	[178,180]

4.2 Subtractive processes

These methods consist of creating small depressions or features by removing the material from the surface[219]. Table XI summarizes the common subtractive routes.

Table XI Classification of the removal of material surface modification techniques[45,219] by subtractive routes

Beam based methods	Laser methods	Laser texturing (LT)
		Masked excimer laser
		Laser honing
		Focused ion beam
		CNC focused laser
		Femtosecond laser
	Electrical discharge machining (EDM)	Electrical discharge texturing (EDT)
		Micro EDM
	Ion beam texturing	
Chemical etching	Masking methods	Chemical texturing
		Electrochemical texturing
	Non-masking methods	Self-assembling
		Maskless laser assisted etching
		Maskless electrochemical texturing
		Anisotropic etching

Mechanical	CNC ultrasonic machining
	Mechanical honing
	Precision Grinding
	Free abrasive machining
	Microcutting
	Patterned erosion

Laser ablation or photoablation rely on using high energy concentrations to ablate the material from a solid (or occasionally liquid) surface by irradiating it with a laser beam. One of the major advantages of this method is that this technique can very conveniently be adopted to process free form surfaces to create surface textures[241,242]. To date, several laser types have been developed such us, excimers, solid state lasers, copper vapour, CO_2, Ti:Sapphire, or diode[243,244]. Moreover, some effects of the laser have been reported such as wavelength, pulse width or scan speed as well as the differences between femtosecond, nanosecond and picosecond[244,245,246,247,248,249,250] pulses. Several studies used femtosecond lasers[46,126,251] and nanosecond lasers[252,253,254,255,256] on different materials to create structured bactericidal surfaces. Figure 31 and Figure 32 show examples of laser structured surfaces reported in the literature.
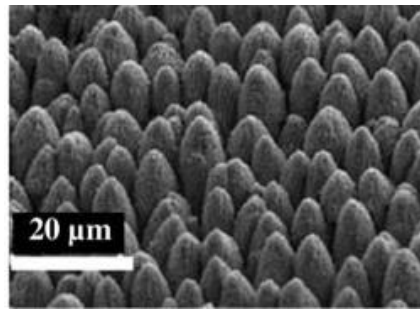

Figure 31: Femtosecond laser processed cone type structure on titanium material. Reproduced with permission from Applied Physics A, 90, 399 (2008) Copyright 2008, Springer [251].
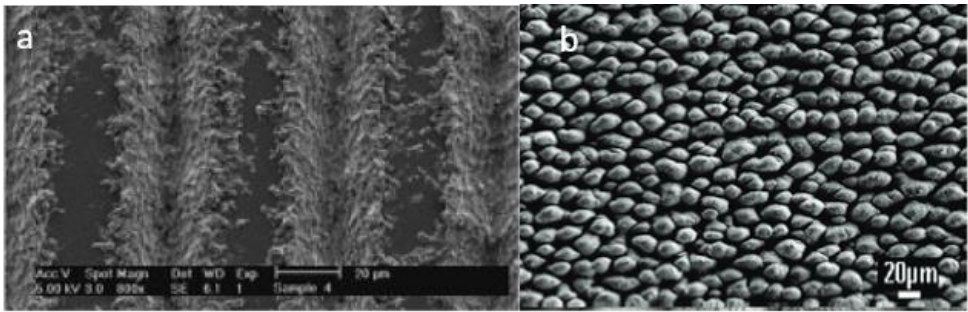
Figure 32 a) Ti6Al4V sample with 50 µm separation tracks. Reproduced with permission from J of Biomed Mat. Research Part B: Applied Biomaterials, 82B, 360 (2007), Copyright 2007, Wiley[254] and b) laser processed titanium sample inspired from a lotus leaf. Reproduced with permission from Langmuir, 27, 3012 (2011), Copyright 2011, ACS[46].

Chen *et al.*[254] fabricated groove like structures with different spacing (Figure 32a) on titanium samples to evaluate the cell response. Unlike laser processing, acid etching relies on immersing the substrates in strong acids such as HCl, H_2SO_4, or HNO_3 to allow material removal from the surface gently[9]. Giner *et al*[257] carried out a study, where titanium discs were cut and etched to study their cell response. It was observed that this method was able to alter the cell response and the contact angle of the surface. Moreover, Zinelis *et al* [258] evaluated the surface properties and elemental alterations produced by EDM on some dental implants. Also, Geim *et al.*[259] fabricated gecko-inspired surfaces using oxygen plasma etching made of polyimide pillars capable of supporting large masses.

Latthe *et al.*[260] reported in their review paper different wettings of the superhydrophobic lotus leaf apart from some techniques used to artificially mimic this surface. Table XII summarises various subtractive routes used in the past for the creation of bactericidal surfaces on different materials and their influence on bacterial activity.

Table XII Subtractive manufacturing processes employed to create bactericidal surfaces

Subtractive process	Materials employed	Bacterial response	Reference
Femtosecond laser	Ti6Al4V	Similar bactericidal (*S. aureus*) response between nanopillars and LIPSS.	126

Femtosecond laser	Ti6Al4V	Colonisation of *S. aureus* on all the laser treated surfaces but rejection of *P. aeruginosa* and *S. mutans* on nanopillar like structure.	[253]
Nanosecond laser	Ti6Al4V	Biofilm formation of *E. coli* and *S. aureus* on non-treated surface but bacterial attachment was not avoided.	[261]
CW laser	Ti6Al4V, CoCrMo and CpTi (Grade 2)	The most bactericidal surface was observed on the CpTi against *S. aureus* which exhibits the lowest CA (31.9°)	[127]
Machining vs Sand blasting + acid etching	Pure Ti	Machined samples showed better bactericidal activity *S. sanguinis* than acid treated ones.	[262]
Polishing vs grit blasting vs plasma sprayed vs satin	Ti6Al4V	Polished surface showed lowest *S. epidermidis* adhesion continued by plasma spraying, grit-blasting and sating.	[108]
Chemical oxidation	Grade 2 Ti	Avoid bacterial adhesion of *S. aureus* and *E. coli* compared to smooth one.	[263]
Plasma glow discharge	PVC	Significant decrease of the *P. aeruginosa* bacteria.	[264]
Plasma treatment	Polymeric suture materials	Reduction of *E. coli* bacteria depends on the available contact area.	[265]

4.3 Re-structuring or patterning

Re-structuring is based on changing the surface structure by plastic deformation and redistribution of material from one part to another. According to Bruzzone et al[219], this stream encompasses various processes as shown in Table XIII.

Table XIII: Classification of the re-structuring surface modification techniques[45,219].

Re-structuring		
Mechanical	Shot blasting	
	Embossing	Vibrorolling
		Patterned embossing tools
		Lithography
		Wrinkling
		Photolithography
Chemical	Molecular migration	
	UV contraction	

During shot blasting, hard small particles impact the substrate at high velocity causing roughening of the surface layer. In this technique, it is difficult to precisely control the texture due to the shape, velocity, and hardness of the particles and the randomness in contact is also difficult to control. It should be noted that shot blasting creates random surfaces[9]. Soboyejo et al.[252] apart from using laser processing, used alumina blasting to modify the surface of a medical device. Bürgers et al.[262] carried out an experiment where samples were modified by blasting with subsequent acid etching and machining. An increase in bacterial adhesion was observed on blasted and subsequently acid-etched samples.

Surface wrinkling is an easy to control fabrication method and one of its advantages is that the surfaces can be easily controlled up to micro/nanoscale[37]. Also, surface wrinkling is characterized by its good tunability and reversibility compared to other patterned techniques[266].

Jiang *et al.*[267] using the lithography surface modification technique created micro-cylinders made of silicon inspired by the lotus leaf. They performed a bacterial test (*E. coli*) to compare a fresh and a silicon lotus leaf. They observed that in the initial 3h of incubation, no bacteria were attached to the surfaces resulting in the advanced hydrophobic property of the surfaces. After 24h of incubation, some bacteria remained attached to the surface, suggesting the air trapped between the microstructure played an essential role in impeding bacterial adhesion.

Also, vibrorolling uses gentle plastic deformation of metals. Usually, a hard metal or a diamond is used to advance into the surface creating uniform texture with regular-shaped asperities.

4.4 Surface property impact of manufacturing techniques

A classification of the most used manufacturing methods for creating bactericidal surfaces and their impact on the surface properties has been made in Table XIV. The final discussion on the metrology aspects of the surfaces is made in the next section.

Table XIV: Impact of the surface properties of different manufacturing techniques.

Technique	Surface property impact				Reference
	Chemistry	Wettability	Topography	Other	
Femtosecond laser	Medium	Strong	Strong (nanoscale, microscale)	No surface damage	46,126,253,268
Nanosecond laser	Medium	Strong	Medium (microscale)	Surface damage	261,269
Ion Implantation	Strong	Weak	Weak	-	179,180
Anodization	Weak	Weak	Weak	-	137
Chemical oxidation	Strong	Strong	Strong (nanoscale)	-	263
PVD	Strong	-	Medium (microscale)	-	229,237
CVD	Strong	Medium	Medium (microscale)	-	240

5. Metrology of precision patterned biomimetic surfaces

This section is dedicated to the measurement or metrology of precision fabricated surfaces. In this section, the most recent and most common surface characterization techniques are briefly reviewed, comparing their functional features and resolutions by identifying advantages and disadvantages that will benefit and facilitate characterisation of bioinspired fabricated surfaces; further information can be found from the relevant sources in the literature[270,271].

Although several techniques are available for surface metrology measurements, most of them use electrons, photons (light), x-ray, ions, or other types of particles or waves, to interact with the surface undergoing testing. In some cases, surface information is derived from tracking the changes induced by the exciting beam. In many others, the information comes from analysing the return signal provided by the samples.

Metrology measurements may require physical contact between probe tips of the measurement device and sample under test, often leading to destruction of the sample's surface, this is called contact metrology. Other methods, mainly optical based, which do not require any physical contact with the samples, are referred to as contactless metrology.
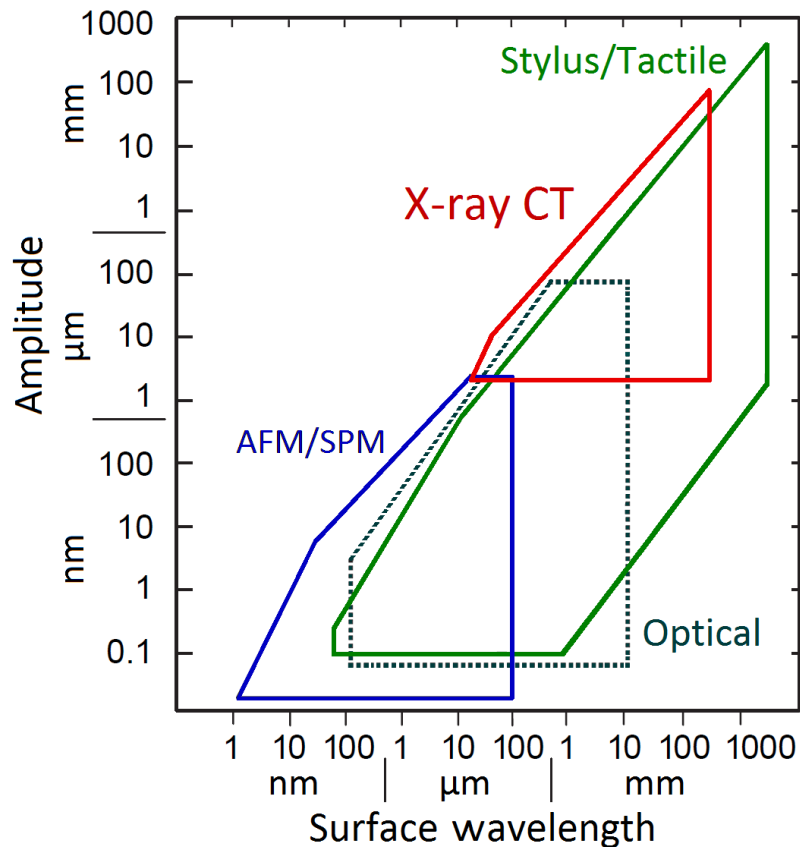
Figure 33: Stedman diagram: Typical resolutions of some common metrology used to assess surface modified fabrication methods. Reproduced with permission from J of Precision Engineering, 64, 228 (2020), Copyright 2020, Elsevier [272].

Figure 33 shows typical specification (resolution) of the most popular and most advanced methods for modified surface metrology measurements involving contact and non-contact modes of measurement in the form of a Stedman diagram[273]. For each characterisation method, there exist many variations (sub-methods) of similar analytical techniques. It is important to emphasize that nowadays the technology is improving rapidly, therefore this illustration can only be used as a reference and not to infer absolute values.

5.1 Contactless metrology

Contactless metrology using optical methods coupled with advanced CCD/CMOS cameras can provide fast measurements on large areas without damaging the surface. However, the resolution of these devices is limited by the wavelength of the electromagnetic radiation used (Rayleigh criterion) and optical aberration, which is the most difficult challenge to overcome in order to reach low resolutions.

Optical microscopes consist of a light source which emits electromagnetic radiation passing through an optical system to project the sample under investigation. The optical systems are designed using different techniques, such as **confocal microscopy** where resolution and contrast are improved by filtering the scattered diffraction, removing the out-of-focus light. Monochromatic confocal microscopes use lasers whereas confocal chromatic systems use white light as the source. Surface information of the sample is extracted by reading and analysing the optical feedback signal from the sample, which could be fluorescence or spectrum of reflected light. The most advanced confocal microscope can reach 0.1 µm depth resolution over a 1 mm measurement range (Figure 33). The optical microscope remains one of the most useful and cost-effective tools for surface metrology in terms of measurement speed, effectiveness and versatility of use.

Optical profiler is a contactless, vertical scanning, white light or laser interferometer which can be used to characterise and quantify surface roughness, height distribution, or other topographical features. It can use 2D or 3D operation with depth resolution ranging from ~1 nm to 5000 µm, and ~10 µm/s scanning speed.

Scanning electron microscopes (SEM) operate with a similar principle to optical microscopes, but instead of using an optical beam (laser or white light), the SEM focuses an electron beam on the sample surface and collects the feedback signal to map the sample surface topography. The feedback signal is normally the number of secondary electrons emitted by the excited atoms of the sample surface. SEM can provide lateral resolution as small as 1 nm. However, as the electron beam must be raster scanned, there is a limit to the sample size, typically < 10 cm. In addition, an electron beam must operate under vacuum so the sample must be compatible with it. From topographical characterization, the major disadvantage is the inability of the conventional SEM to measure in the third dimension, or depth of topographical features. Even though in the past two decades some stereology techniques have been developed to obtain quantitative 3D information[274], it is usually used qualitatively and as a lateral quantity only, rather than as a primary surface measurement instrument.

Dynamic force microscopes, such as Electrostatic Force Microscopes (EFM), are non-contact but not optical based methods. In EFM, a cantilever sensor tip is held at ~1 to 100 nm from the sample surface. This distance is large enough to avoid collision between the tip and the sample's surface. Applying a biased voltage (AC or DC) between the conductive cantilever and the sample can create an electrostatic force that can be probed and mapped while scanning the sensor tip over the surface of the sample. EFM is a promising method for sub-micrometric surface measurements but it works only with electrically conducting samples making it appropriate for characterising medical implants.

5.2 Contact metrology

Contact metrology may have better resolution than contactless methods, but this approach often leads to small scale plastic deformation (of destructive nature) on the sample surface intended to be measured.

For the characterization of surface topography at the nanometer level, Atomic Force Microscope (AFM) is a powerful tool. It consists of a probe tip of a nanometer size located at the free end of a cantilever. When the tip approaches the sample surface, it reaches a critical distance as small as the atomic level (a few angstroms), resulting in the cantilever experiencing a bending force arising from van der Waals forces. This bending level can be measured by a position-sensitive detector. Unlike EFM, AFM does not measure the tunnelling current between the probe tip and the surface, instead it measures the direct

interaction at the atomic level between the two, and hence is a contact measurement method. The lateral resolutions of an AFM depend on the size of the probe tip, typically < 1 nm, whereas the depth resolution depends on the sensitivity of the position sensitive detection, which could be as small as 0.1 nm.

A stylus profiler is typically a one-and-a-half-dimension coordinate measurement machine which operates based on the mechanical principle. It is very useful for surface roughness and topography measurements because its measurement range is very large. It consists of a stylus with a micrometer or sub-micrometer probe tip which moves up and down while scanning around the sample surface. The sample surface topography information is then reconstructed based on the up and down data measured. This method gives a quick result on almost any type of material.

6. Future research directions and conclusions

The idea of creating antibacterial materials by modifying the surfaces needs to be exploited in more detail. To create new generation advanced medical materials, deep research is required. This review hinted at some possible future research endeavours that future researchers could benefit from.

Firstly, it was observed that the effect of chemistry, in section 3.3, repulsing bacterial adhesion has a minor effect. Nevertheless, it has been reported that removing wax from the lotus leaf, in section 2.2.1 from the surface has a significant impact on the surface hydrophobicity. Thus, more studies are required to clarify the effect of surface chemistry on bacterial adhesion. From the literature on this topic, we also noticed some contradictory results, for example, Yang and Deng[133] reported that hydrophobic surfaces prevent bacterial adhesion whereas Cunha et al[126] reported that hydrophilic surfaces avoid bacterial adhesion.

No direct evidence was found in support of the argument that the wetting angle has a direct correlation to bacterial attachment. Certainly, a wetting contact angle speaks to the surface energy, but this review asks a key question, can this alone describe the nature of bacterial attachment? This review highlighted that in some cases a change in the contact wetting angle on the surface may not necessarily confirm that the surface is bactericidal and biological laboratory tests would be required to unambiguously prove that the modified surface is bactericidal.

What was also learned from this review was that most of the cartoon models explaining the bacterial killing from the spikes on the surfaces assume the bacteria to be isolated from the environment, whereas in reality a bacterial testing process is carried out in a broth to provide nutrients to the bacteria and while some bacteria are killed by the bactericidal surfaces the other bacteria in the broth keep proliferating. Thus, fabricating a bactericidal surface capable of killing all bacteria in the broth at once is unlikely and current models do not capture this aspect. This knowledge gap mandates the necessity of undertaking laboratory-scale, pre-clinical and post-clinical examination of the bactericidal surfaces. The only thing that may be speculated is that the surfaces should aim at suppressing the probability of bacterial infection. Complete eradication of bacterial growth by making nature-inspired fabricated surfaces is merely a hypothesis.

The published literature available on bactericidal surfaces does discuss the influence of surface roughness on bacterial attachment i.e. the parameter average surface roughness (Ra) can be misleading and more work is required to establish a concrete correlation between surface topography and bacterial adhesion. It was highlighted that the two-dimensional Ra parameter is insufficient for describing the surface topography. The introduction of 3D surface characterization parameters is necessary to provide a richer set of surface descriptors. It is anticipated that this could provide a correlation with bactericidal effects. The challenge remains in the creation of these special hierarchical structured surfaces. Some of these structured surfaces require manipulation at multiple length scales and combining different scales on the same surface remains the most ambitious challenge in the manufacturing process.

This review highlighted the growing need for identifying materials and manufacturing solutions for scalable fabrication of patterned hierarchical structures that are demonstrated to be bactericidal. Production of nature-inspired nanostructured surfaces exhibiting dimensions of the order of a few nanometres (this limit is set by the size of the bacteria ~ typically about 1 to 2 micron diameter for staphylococci) on the complex freeform medical implant materials is proposed to be a major 21st Century challenge as it involves multidisciplinary efforts ranging from manufacturing, materials, surface science and biology disciplines to name a few.

Currently available commercial medical implants do not have the functionalities required to offset the formation of the biofilm that contributes to the infection. The cost-laden repeated surgeries, as a result, directly contribute to a significant cost burden on the

national economy in a growing ageing society. This review shows that nature is a good inspiration to capture nanostructures that have resulted in many millennia of evolution, and their integration into new generations of products, vis-à-vis hierarchical structures is the key to achieve bactericidal surfaces. The most efficient and promising bactericidal surfaces were reviewed, and dragonfly wings or cicada wings were found to be exceptionally well-suited examples.

It was concluded that the topography, wettability and the chemistry of the surface are the critical aspects to consider in achieving the bactericidal surfaces and the slope presented by these surfaces can allow machine learning to design functional surfaces hitherto not known to provide unique functionality.

Besides bactericidal surfaces, various ultra-precision manufacturing and metrology routes are reviewed in great length with a focus on using these methods for fabricating bactericidal surfaces in a scalable way. Femtosecond laser machining here appears as the possible solution for the futuristic products. It was finally concluded that to mimic precisely natural surfaces, the ultra-precision manufacturing society needs to develop a radically new concept to produce scalable fabrication routes for the nature-inspired surfaces and this journey seems to go via the path of "Precision additive manufacturing" (PAM), a technology that has yet to be fully developed but holds the key to the future of ultra-precision manufacturing.

Acknowledgments

Data Statement

All data in the manuscript will be available through Cranfield University open repository 10.17862/cranfield.rd.12925706

References

[1] S. Goel, S. Hawi, G. Goel, V.K. Thakur, A. Agrawal, C. Hoskins, O. Pearce, T. Hussain, H.M. Upadhyaya, G. Cross, and A.H. Barber, Mater. Today Chem. **17**, 100300 (2020).

[2] D. Adamovic, B. Ristic, and F. Zivic, in *Biomater. Clin. Pract. Adv. Clin. Res. Med. Devices* (Springer International Publishing, 2017), pp. 47–99.

[3] W.F. Oliveira, P.M.S. Silva, R.C.S. Silva, G.M.M. Silva, G. Machado, L.C.B.B. Coelho, and M.T.S. Correia, J. Hosp. Infect. **98**, 111 (2018).

[4] C.R. Arciola, D. Campoccia, and L. Montanaro, Nat. Rev. Microbiol. **16**, 397 (2018).

[5] S. Veerachamy, T. Yarlagadda, G. Manivasagam, and P.K. Yarlagadda, Proc. Inst. Mech. Eng. Part H J. Eng. Med. **228**, 1083 (2014).

[6] J.W. Costerton, L. Montanaro, and C.R. Arciola, Int. J. Artif. Organs **28**, 1062 (2005).

[7] (n.d.).

[8] Y. Kirmanidou, M. Sidira, M.E. Drosou, V. Bennani, A. Bakopoulou, A. Tsouknidas, N. Michailidis, and K. Michalakis, Biomed Res. Int. **2016**, (2016).

[9] X. Liu, P.K. Chu, and C. Ding, Mater. Sci. Eng. R Reports **47**, (2004).

[10] A. Tripathy, P. Sen, B. Su, and W.H. Briscoe, Adv. Colloid Interface Sci. **248**, 85 (2017).

[11] L. Feng, S. Li, Y. Li, H. Li, L. Zhang, J. Zhai, Y. Song, B. Liu, L. Jiang, and D. Zhu, Adv. Mater. **14**, 1857 (2002).

[12] G.S. Watson, D.W. Green, L. Schwarzkopf, X. Li, B.W. Cribb, S. Myhra, and J.A. Watson, Acta Biomater. **21**, 109 (2015).

[13] B. Bhushan and Y.C. Jung, Prog. Mater. Sci. **56**, 1 (2011).

[14] X. Zhang, L. Wang, and E. Levänen, RSC Adv. **3**, 12003 (2013).

[15] C.D. Bandara, S. Singh, I.O. Afara, A. Wolff, T. Tesfamichael, K. Ostrikov, and A. Oloyede, ACS Appl. Mater. Interfaces **9**, 6746 (2017).

[16] A.T. Poortinga, R. Bos, W. Norde, and H.J. Busscher, Surf. Sci. Rep. **47**, (2002).

[17] M. Hermansson, Colloids Surfaces B Biointerfaces **14**, (1999).

[18] C. Desrousseaux, V. Sautou, S. Descamps, and O. Traoré, J. Hosp. Infect. **85**, 87 (2013).

[19] E. O'Neill, C. Pozzi, P. Houston, H. Humphreys, D.A. Robinson, A. Loughman, T.J. Foster, and J.P. O'Gara, J. Bacteriol. **190**, 3835 (2008).

[20] C. Berne, A. Ducret, G.G. Hardy, and Y. V. Brun, in *Microb. Biofilms* (ASM Press, Washington, DC, USA, 2015), pp. 163–199.

[21] R.M. Donlan, in *Emerg. Infect. Dis.* (Centers for Disease Control and Prevention (CDC), 2001), pp. 277–281.

[22] D. Lindsay and A. von Holy, J. Hosp. Infect. **64**, 313 (2006).

[23] S.C. Cortelli, J.R. Cortelli, R.L. Romeiro, F.O. Costa, D.R. Aquino, P.R. Orzechowski, V.C. Araújo, and P.M. Duarte, Arch. Oral Biol. **58**, 67 (2013).

[24] R. Wasfi, S.M. Hamed, M.A. Amer, and L.I. Fahmy, Front. Cell. Infect. Microbiol. **10**, 414 (2020).

[25] H. Anwar, M.K. Dasgupta, and J.W. Costerton, Antimicrob. Agents Chemother. **34**,

2043 (1990).

[26] K.L. Mittal, *Contact Angle, Wettability and Adhesion, Volume 5* (2008).

[27] A. Cunha, *Multiscale Femtosecond Laser Surface Texturing of Titanium and Titanium Alloys for Dental and Medical Orthopaedic Implants* (Bordeaux, 2015).

[28] T. Sun, L. Feng, X. Gao, and L. Jiang, Acc. Chem. Res. **38**, 644 (2005).

[29] K. Koch, B. Bhushan, and W. Barthlott, Prog. Mater. Sci. **54**, 137 (2009).

[30] K. Koch, B. Bhushan, and W. Barthlott, Soft Matter **4**, 1943 (2008).

[31] A. Malshe, K. Rajurkar, A. Samant, H.N. Hansen, S. Bapat, and W. Jiang, CIRP Ann. - Manuf. Technol. **62**, 607 (2013).

[32] J. Genzer and K. Efimenko, Biofouling **22**, 339 (2006).

[33] A. Marmur, Biofouling **22**, 107 (2006).

[34] A.B.D. Cassie and S. Baxter, Trans. Faraday Soc. **40**, 546 (1944).

[35] D. Patel, V. Jain, and J. Ramkumar, Proc. Inst. Mech. Eng. Part B J. Eng. Manuf. **232**, 941 (2018).

[36] G. Carbone and L. Mangialardi, Eur. Phys. J. E **16**, 67 (2005).

[37] J. Sun and B. Bhushan, Tribol. Int. **129**, 67 (2019).

[38] J. Hasan, R.J. Crawford, and E.P. Ivanova, Trends Biotechnol. **31**, 295 (2013).

[39] S. Nishimoto and B. Bhushan, RSC Adv. **3**, 671 (2013).

[40] W. Barthlott and C. Neinhuis, Planta **202**, 1 (1997).

[41] P.Y. Chen, J. McKittrick, and M.A. Meyers, Prog. Mater. Sci. **57**, (2012).

[42] K. Koch, B. Bhushan, Y.C. Jung, and W. Barthlott, Soft Matter **5**, 1386 (2009).

[43] H.J. Ensikat, P. Ditsche-Kuru, C. Neinhuis, and W. Barthlott, Beilstein J. Nanotechnol. **2**, 152 (2011).

[44] B. Bhushan, Philos. Trans. R. Soc. A Math. Phys. Eng. Sci. **367**, 1445 (2009).

[45] A. Jaggessar, H. Shahali, A. Mathew, and P.K.D.V. Yarlagadda, J. Nanobiotechnology **15**, 1 (2017).

[46] E. Fadeeva, V.K. Truong, M. Stiesch, B.N. Chichkov, R.J. Crawford, J. Wang, and E.P. Ivanova, Langmuir **27**, 3012 (2011).

[47] Y.Y. Yan, N. Gao, and W. Barthlott, Adv. Colloid Interface Sci. **169**, 80 (2011).

[48] L.P. Biró, Mater. Sci. Eng. B Solid-State Mater. Adv. Technol. **169**, 3 (2010).

[49] V. Saranathan, C.O. Osuji, S.G.J. Mochrie, H. Noh, S. Narayanan, A. Sandy, E.R. Dufresne, and R.O. Prum, Proc. Natl. Acad. Sci. U. S. A. **107**, 11676 (2010).

[50] P. Vukusic, J.R. Sambles, C.R. Lawrence, and R.J. Wootton, Proc. R. Soc. London. Ser. B Biol. Sci. **266**, 1403 (1999).

[51] Y. Ding, S. Xu, and Z.L. Wang, J. Appl. Phys. **106**, 074702 (2009).

[52] S. Yoshioka and S. Kinoshita, Proc. R. Soc. London. Ser. B Biol. Sci. **271**, 581 (2004).

[53] Y. Zheng, X. Gao, and L. Jiang, Soft Matter **3**, 178 (2007).

[54] D.Y. Zhao, Z.P. Huang, M.J. Wang, T. Wang, and Y. Jin, J. Mater. Process. Technol. **212**, 198 (2012).

[55] K.K. Chung, J.F. Schumacher, E.M. Sampson, R.A. Burne, P.J. Antonelli, and A.B. Brennan, Biointerphases **2**, 89 (2007).

[56] J.F. Schumacher, M.L. Carman, T.G. Estes, A.W. Feinberg, L.H. Wilson, M.E. Callow, J.A. Callow, J.A. Finlay, and A.B. Brennan, Biofouling **23**, 55 (2007).

[57] J.F. Schumacher, N. Aldred, M.E. Callow, J.A. Finlay, J.A. Callow, A.S. Clare, and A.B. Brennan, Biofouling **23**, 307 (2007).

[58] V. Tinnemann, L. Hernández, S.C.L. Fischer, E. Arzt, R. Bennewitz, and R. Hensel, Adv. Funct. Mater. **29**, 1807713 (2019).

[59] B. Bhushan, J. Adhes. Sci. Technol. **21**, 1213 (2007).

[60] W.R. Hansen and K. Autumn, Proc. Natl. Acad. Sci. U. S. A. **102**, 385 (2005).

[61] K. Autumn, Y.A. Liang, S.T. Hsieh, W. Zesch, W.P. Chan, T.W. Kenny, R. Fearing, and R.J. Full, Nature **405**, (2000).

[62] X. Li, G.S. Cheung, G.S. Watson, J.A. Watson, S. Lin, L. Schwarzkopf, and D.W. Green, Nanoscale **8**, 18860 (2016).

[63] E.P. Ivanova, J. Hasan, H.K. Webb, V.K. Truong, G.S. Watson, J.A. Watson, V.A. Baulin, S. Pogodin, J.Y. Wang, M.J. Tobin, C. Löbbe, and R.J. Crawford, Small **8**, 2489 (2012).

[64] G.S. Watson, S. Myhra, B.W. Cribb, and J.A. Watson, Biophys. J. **94**, 3352 (2008).

[65] J. Hasan, H.K. Webb, V.K. Truong, S. Pogodin, V.A. Baulin, G.S. Watson, J.A. Watson, R.J. Crawford, and E.P. Ivanova, Appl. Microbiol. Biotechnol. **97**, 9257 (2013).

[66] S. Pogodin, J. Hasan, V.A. Baulin, H.K. Webb, V.K. Truong, T.H. Phong Nguyen, V. Boshkovikj, C.J. Fluke, G.S. Watson, J.A. Watson, R.J. Crawford, and E.P. Ivanova, Biophys. J. **104**, 835 (2013).

[67] J. Román-Kustas, J.B. Hoffman, J.H. Reed, A.E. Gonsalves, J. Oh, L. Li, S. Hong, K.D. Jo, C.E. Dana, N. Miljkovic, D.M. Cropek, and M. Alleyne, Adv. Mater. Interfaces **7**, 2000112 (2020).

[68] D.E. Mainwaring, S.H. Nguyen, H. Webb, T. Jakubov, M. Tobin, R.N. Lamb, A.H.F. Wu, R. Marchant, R.J. Crawford, and E.P. Ivanova, Nanoscale **8**, 6527 (2016).

[69] C.M. Bhadra, V. Khanh Truong, V.T.H. Pham, M. Al Kobaisi, G. Seniutinas, J.Y. Wang, S. Juodkazis, R.J. Crawford, and E.P. Ivanova, Sci. Rep. **5**, 16817 (2015).

[70] K. Modaresifar, S. Azizian, M. Ganjian, L.E. Fratila-Apachitei, and A.A. Zadpoor, Acta Biomater. **83**, 29 (2019).

[71] A.A. Voevodin and J.S. Zabinski, Thin Solid Films **370**, (2000).

[72] J. Teyssier, S. V. Saenko, D. Van Der Marel, and M.C. Milinkovitch, Nat. Commun. **6**, (2015).

[73] M. Spinner, G. Westhoff, and S.N. Gorb, Sci. Rep. **4**, 1 (2014).

[74] H.H. Chou, A. Nguyen, A. Chortos, J.W.F. To, C. Lu, J. Mei, T. Kurosawa, W.G. Bae, J.B.H. Tok, and Z. Bao, Nat. Commun. **6**, 1 (2015).

[75] M. Vatankhah-Varnosfaderani, A.N. Keith, Y. Cong, H. Liang, M. Rosenthal, M. Sztucki, C. Clair, S. Magonov, D.A. Ivanov, A. V. Dobrynin, and S.S. Sheiko, Science (80-.). **359**, 1509 (2018).

[76] K.B. Karsten, G.W. Ferguson, T. Chen, and M.F. Holick, Physiol. Biochem. Zool. **82**, 218 (2009).

77 H. Toyota, K. Takahara, M. Okano, T. Yotsuya, and H. Kikuta, Japanese J. Appl. Physics, Part 2 Lett. **40**, L747 (2001).

78 J. Aizenberg, A. Tkachenko, S. Weiner, L. Addadi, and G. Hendler, Nature **412**, (2001).

79 P.B. Applewhite, Behav. Biol. **7**, (1972).

80 H.S. Patil and S. Vaijapurkar, J. Bionic Eng. **4**, 19 (2007).

81 M. Ueda, H. Shigemori, N. Sata, and S. Yamamura, Phytochemistry **53**, (2000).

82 H. Lowenstam and S. Weiner, *On Biomineralization* (Oxford University Press, 1989).

83 D.R. Talham, Cryst. Growth Des. **2**, (2002).

84 J. Moradian-Oldak, H.B. Wen, G.B. Schneider, and C.M. Stanford, Periodontol. 2000 **41**, 157 (2006).

85 P. Lucas, P. Constantino, B. Wood, and B. Lawn, BioEssays **30**, 374 (2008).

86 P. Vukusic and J.R. Sambles, Nature **424**, (2003).

87 A.. Ingram and A.. Parker, Philos. Trans. R. Soc. B Biol. Sci. **363**, 2465 (2008).

88 S. Kinoshita and S. Yoshioka, ChemPhysChem **6**, 1442 (2005).

89 P. Vukusic and I. Hooper, Science (80-.). **310**, 1151 (2005).

90 S.C. Burgess, A. King, and R. Hyde, in *Opt. Laser Technol.* 38, 329 (2006).

91 J. Zi, X. Yu, Y. Li, X. Hu, C. Xu, X. Wang, X. Liu, and R. Fu, Proc. Natl. Acad. Sci. U. S. A. **100**, 12576 (2003).

92 L. D'Alba, V. Saranathan, J.A. Clarke, J.A. Vinther, R.O. Prum, and M.D. Shawkey, Biol. Lett. **7**, 543 (2011).

93 G.S. Watson, D.W. Green, B.W. Cribb, C.L. Brown, C.R. Meritt, M.J. Tobin, J. Vongsvivut, M. Sun, A.P. Liang, and J.A. Watson, ACS Appl. Mater. Interfaces **9**, 24381 (2017).

94 X. Pu, G. Li, and Y. Liu, ChemBioEng Rev. **3**, 26 (2016).

95 D.W. Green, K.K.H. Lee, J.A. Watson, H.Y. Kim, K.S. Yoon, E.J. Kim, J.M. Lee, G.S. Watson, and H.S. Jung, Sci. Rep. **7**, (2017).

[96] G.S. Watson, J.A. Watson, S. Hu, C.L. Brown, B.W. Cribb, and S. Myhra, Int. J. Nanomanuf. **5**, 112 (2010).

[97] E.P. Ivanova, J. Hasan, H.K. Webb, G. Gervinskas, S. Juodkazis, V.K. Truong, A.H.F. Wu, R.N. Lamb, V.A. Baulin, G.S. Watson, J.A. Watson, D.E. Mainwaring, and R.J. Crawford, Nat. Commun. **4**, (2013).

[98] R. Selvakumar, K.K. Karuppanan, and R. Pezhinkattil, Micron **43**, 1299 (2012).

[99] J. Hasan, S. Raj, L. Yadav, and K. Chatterjee, RSC Adv. **5**, (2015).

[100] T. Diu, N. Faruqui, T. Sjöström, B. Lamarre, H.F. Jenkinson, B. Su, and M.G. Ryadnov, Sci. Rep. **4**, (2014).

[101] C. Sengstock, M. Lopian, Y. Motemani, A. Borgmann, C. Khare, P.J.S. Buenconsejo, T.A. Schildhauer, A. Ludwig, and M. Köller, Nanotechnology **25**, 195101 (2014).

[102] G. Zhang, J. Zhang, G. Xie, Z. Liu, and H. Shao, Small **2**, 1440 (2006).

[103] T. Sjöström, A.H. Nobbs, and B. Su, Mater. Lett. **167**, 22 (2016).

[104] V.K. Truong, H.K. Webb, E. Fadeeva, B.N. Chichkov, A.H.F. Wu, R. Lamb, J.Y. Wang, R.J. Crawford, and E.P. Ivanova, Biofouling **28**, 539 (2012).

[105] A. Sakamoto, Y. Terui, C. Horie, T. Fukui, T. Masuzawa, S. Sugawara, K. Shigeta, T. Shigeta, K. Igarashi, and K. Kashiwagi, FEMS Microbiol. Lett. **361**, 10 (2014).

[106] D.W. Bechert, M. Bruse, and W. Hage, Exp. Fluids **28**, (2000).

[107] E.E. Mann, M.R. Mettetal, R.M. May, M.C. Drinker, B.C. Stevenson, V.L. Baiamonte, J.M. Marso, E.A. Dannemiller, A.E. Parker, and S.T. Reddy, J. Microbiol. Exp. **1**, 32 (2014).

[108] Y. Wu, J.P. Zitelli, K.S. TenHuisen, X. Yu, and M.R. Libera, Biomaterials **32**, 951 (2011).

[109] V.K. Truong, R. Lapovok, Y.S. Estrin, S. Rundell, J.Y. Wang, C.J. Fluke, R.J. Crawford, and E.P. Ivanova, Biomaterials **31**, 3674 (2010).

[110] E.P. Ivanova, V.K. Truong, H.K. Webb, V.A. Baulin, J.Y. Wang, N. Mohammodi, F. Wang, C. Fluke, and R.J. Crawford, Sci. Rep. **1**, 1 (2011).

[111] F. Aykent, I. Yondem, A.G. Ozyesil, S.K. Gunal, M.C. Avunduk, and S. Ozkan, J.

Prosthet. Dent. **103**, 221 (2010).

[112] R.L. Taylor, J. Verran, G.C. Lees, and A.J.P. Ward, J. Mater. Sci. Mater. Med. **9**, 17 (1998).

[113] E.W. McAllister, L.C. Carey, P.G. Brady, R. Heller, and S.G. Kovacs, Gastrointest. Endosc. **39**, (1993).

[114] L.. Baker, A.S; Greenham, J. Bone Joint Surg. Am. (1988).

[115] L.R. Hilbert, D. Bagge-Ravn, J. Kold, and L. Gram, Int. Biodeterior. Biodegrad. **52**, (2003).

[116] I. Yoda, H. Koseki, M. Tomita, T. Shida, H. Horiuchi, H. Sakoda, and M. Osaki, BMC Microbiol. **14**, 234 (2014).

[117] R.J. Crawford, H.K. Webb, V.K. Truong, J. Hasan, and E.P. Ivanova, Adv. Colloid Interface Sci. **179**–**182**, 142 (2012).

[118] A. Zabala, L. Blunt, W. Tato, A. Aginagalde, X. Gomez, and I. Llavori, in *MATEC Web Conf.* (EDP Sciences, 2018), p. 14013.

[119] B. Ercan, E. Taylor, E. Alpaslan, and T.J. Webster, Nanotechnology **22**, 295102 (2011).

[120] W.-Q. Yu, X.-Q. Jiang, L. Xu, Y.-F. Zhao, F.-Q. Zhang, and X. Cao, J. Biomed. Mater. Res. Part B Appl. Biomater. **99B**, 207 (2011).

[121] A.I. Hochbaum and J. Aizenberg, Nano Lett. **10**, 3717 (2010).

[122] M. Lorenzetti, I. Dogša, T. Stošicki, D. Stopar, M. Kalin, S. Kobe, and S. Novak, ACS Appl. Mater. Interfaces **7**, (2015).

[123] K. Anselme, P. Davidson, A.M. Popa, M. Giazzon, M. Liley, and L. Ploux, Acta Biomater. **6**, 3824 (2010).

[124] S. Wu, F. Zuber, K. Maniura-Weber, J. Brugger, and Q. Ren, J. Nanobiotechnology **16**, 1 (2018).

[125] X. Li and T. Chen, Phys. Rev. E **93**, 052419 (2016).

[126] A. Cunha, A.M. Elie, L. Plawinski, A.P. Serro, A.M. Botelho Do Rego, A. Almeida, M.C. Urdaci, M.C. Durrieu, and R. Vilar, Appl. Surf. Sci. **360**, 485 (2016).

[127] C.W. Chan, L. Carson, G.C. Smith, A. Morelli, and S. Lee, Appl. Surf. Sci. **404**, 67 (2017).

[128] Y.H. An and R.J. Friedman, J. Biomed. Mater. Res. **43**, 338 (1998).

[129] S.D. Puckett, E. Taylor, T. Raimondo, and T.J. Webster, Biomaterials **31**, 706 (2010).

[130] L.G. Harris and R.G. Richards, Injury **37**, (2006).

[131] C. Lin, P. Tang, W. Zhang, Y. Wang, B. Zhang, H. Wang, and L. Zhang, J. Nanomater. **2011**, (2011).

[132] J.H. Lee, G. Khang, J.W. Lee, and H.B. Lee, J. Colloid Interface Sci. **205**, (1998).

[133] H. Yang and Y. Deng, J. Colloid Interface Sci. **325**, 588 (2008).

[134] D. Campoccia, L. Montanaro, H. Agheli, D.S. Sutherland, V. Pirini, M.E. Donati, and C.R. Arciola, Int. J. Artif. Organs **29**, 622 (2006).

[135] L. Visai, L. de Nardo, C. Punta, L. Melone, A. Cigada, M. Imbriani, and C.R. Arciola, Int. J. Artif. Organs **34**, 929 (2011).

[136] B. Del Curto, M.F. Brunella, C. Giordano, M.P. Pedeferri, V. Valtulina, L. Visai, and A. Cigada, Int. J. Artif. Organs **28**, 718 (2005).

[137] C. Giordano, E. Saino, L. Rimondini, M.P. Pedeferri, L. Visai, A. Cigada, and R. Chiesa, Colloids Surfaces B Biointerfaces **88**, 648 (2011).

[138] C.C. Chu and D.F. Williams, Am. J. Surg. **147**, (1984).

[139] M.J. Hajipour, K.M. Fromm, A. Akbar Ashkarran, D. Jimenez de Aberasturi, I.R. de Larramendi, T. Rojo, V. Serpooshan, W.J. Parak, and M. Mahmoudi, Trends Biotechnol. **30**, 499 (2012).

[140] S.Y. Liau, D.C. Read, W.J. Pugh, J.R. Furr, and A.D. Russell, Lett. Appl. Microbiol. **25**, 279 (1997).

[141] J.R. Morones, J.L. Elechiguerra, A. Camacho, K. Holt, J.B. Kouri, J.T. Ramírez, and M.J. Yacaman, Nanotechnology **16**, 2346 (2005).

[142] I. Sondi and B. Salopek-Sondi, J. Colloid Interface Sci. **275**, (2004).

[143] X.H.N. Xu, W.J. Brownlow, S. V. Kyriacou, Q. Wan, and J.J. Viola, Biochemistry **43**,

10400 (2004).

[144] G. Borkow and J. Gabbay, Curr. Chem. Biol. **3**, 272 (2009).

[145] A.K. Chatterjee, R. Chakraborty, and T. Basu, Nanotechnology **25**, 135101 (2014).

[146] L.F. Espinosa-Cristóbal, G.A. Martínez-Castañón, R.E. Martínez-Martínez, J.P. Loyola-Rodríguez, N. Patiño-Marín, J.F. Reyes-Macías, and F. Ruiz, Mater. Lett. **63**, 2603 (2009).

[147] L. Juan, Z. Zhimin, M. Anchun, L. Lei, and Z. Jingchao, Int. J. Nanomedicine **5**, 261 (2010).

[148] L. Zhao, H. Wang, K. Huo, L. Cui, W. Zhang, H. Ni, Y. Zhang, Z. Wu, and P.K. Chu, Biomaterials **32**, 5706 (2011).

[149] A. Mo, J. Liao, W. Xu, S. Xian, Y. Li, and S. Bai, Appl. Surf. Sci. **255**, 435 (2008).

[150] R. Sinha, R. Karan, A. Sinha, and S.K. Khare, Bioresour. Technol. **102**, 1516 (2011).

[151] S. Parham, D.H.B. Wicaksono, S. Bagherbaigi, S.L. Lee, and H. Nur, J. Chinese Chem. Soc. **63**, 385 (2016).

[152] Y.N. Slavin, J. Asnis, U.O. Häfeli, and H. Bach, J. Nanobiotechnology **15**, 65 (2017).

[153] S.M. Dizaj, F. Lotfipour, M. Barzegar-Jalali, M.H. Zarrintan, and K. Adibkia, Mater. Sci. Eng. C **44**, 278 (2014).

[154] S. Stankic, S. Suman, F. Haque, and J. Vidic, J. Nanobiotechnology **14**, 73 (2016).

[155] H. Qin, H. Cao, Y. Zhao, G. Jin, M. Cheng, J. Wang, Y. Jiang, Z. An, X. Zhang, and X. Liu, ACS Appl. Mater. Interfaces **7**, 10785 (2015).

[156] S. Mei, H. Wang, W. Wang, L. Tong, H. Pan, C. Ruan, Q. Ma, M. Liu, H. Yang, L. Zhang, Y. Cheng, Y. Zhang, L. Zhao, and P.K. Chu, Biomaterials **35**, 4255 (2014).

[157] Y. Zheng, J. Li, X. Liu, and J. Sun, Int. J. Nanomedicine **7**, 875 (2012).

[158] T. Zdziech, M. Hajduga, and D. Jedrzejczyk, in *Met. 2012 - Conf. Proceedings, 21st Int. Conf. Metall. Mater.* (2012).

[159] Y. Zhu, H. Cao, S. Qiao, M. Wang, Y. Gu, H. Luo, F. Meng, X. Liu, and H. Lai, Int. J. Nanomedicine **10**, 6659 (2015).

[160] G. Jin, H. Qin, H. Cao, S. Qian, Y. Zhao, X. Peng, X. Zhang, X. Liu, and P.K. Chu, Biomaterials **35**, 7699 (2014).

[161] H. Cao, W. Zhang, F. Meng, J. Guo, D. Wang, S. Qian, X. Jiang, X. Liu, and P.K. Chu, ACS Appl. Mater. Interfaces **9**, 5149 (2017).

[162] I. Lampé, D. Beke, S. Biri, I. Csarnovics, A. Csik, Z. Dombrádi, P. Hajdu, V. Hegedűs, R. Rácz, I. Varga, and C. Hegedűs, Int. J. Nanomedicine **14**, 4709 (2019).

[163] G. Wang, W. Jin, A.M. Qasim, A. Gao, X. Peng, W. Li, H. Feng, and P.K. Chu, Biomaterials **124**, 25 (2017).

[164] C. Zhu, N.R. Bao, S. Chen, and J.N. Zhao, Appl. Surf. Sci. **389**, 7 (2016).

[165] X. Hou, D. Mao, H. Ma, Y. Ai, X. Zhao, J. Deng, D. Li, and B. Liao, Mater. Lett. **161**, 309 (2015).

[166] X. Hou, H. Ma, F. Liu, J. Deng, Y. Ai, X. Zhao, D. Mao, D. Li, and B. Liao, J. Hazard. Mater. **299**, 59 (2015).

[167] S. Qiao, H. Cao, X. Zhao, H. Lo, L. Zhuang, Y. Gu, J. Shi, X. Liu, and H. Lai, Int. J. Nanomedicine **10**, 653 (2015).

[168] J. Osés, J.F. Palacio, S. Kulkarni, A. Medrano, J.A. García, and R. Rodríguez, Appl. Surf. Sci. **310**, 56 (2014).

[169] P. Zhang, Z. Zhang, and W. Li, J. Nanomater. **2013**, (2013).

[170] R. Chen, H. Ni, H. Zhang, G. Yue, W. Zhan, and P. Xiong, in *Vacuum* (Pergamon, 2013), pp. 249–253.

[171] H. Cao, X. Liu, F. Meng, and P.K. Chu, Biomaterials **32**, 693 (2011).

[172] J. Zhao, H.J. Feng, H.Q. Tang, and J.H. Zheng, Surf. Coatings Technol. **201**, (2007).

[173] H.Q. Tang, T. Liu, X. Liu, H.Q. Gu, and J. Zhao, Nucl. Instruments Methods Phys. Res. Sect. B Beam Interact. with Mater. Atoms **255**, (2007).

[174] G. Jin, H. Qin, H. Cao, Y. Qiao, Y. Zhao, X. Peng, X. Zhang, X. Liu, and P.K. Chu, Biomaterials **65**, 22 (2015).

[175] H. Cao, T. Cui, G. Jin, and X. Liu, Surf. Coatings Technol. **256**, 9 (2014).

[176] R. Huang, Y. Han, and S. Lu, J. Mater. Chem. B **2**, 4531 (2014).

[177] H.W. Ni, H.S. Zhang, R.S. Chen, W.T. Zhan, K.F. Huo, and Z.Y. Zuo, Int. J. Miner. Metall. Mater. **19**, (2012).

[178] J. Fiedler, A. Kolitsch, B. Kleffner, D. Henke, S. Stenger, and R.E. Brenner, Int. J. Artif. Organs **34**, 882 (2011).

[179] W. Zhang and P.K. Chu, Surf. Coatings Technol. **203**, (2008).

[180] Y.Z. Wan, S. Raman, F. He, and Y. Huang, Vacuum **81**, (2007).

[181] J. Vetter, Surf. Coatings Technol. **257**, 213 (2014).

[182] K. Bewilogua and D. Hofmann, Surf. Coatings Technol. **242**, 214 (2014).

[183] R. Hauert, K. Thorwarth, and G. Thorwarth, Surf. Coatings Technol. **233**, 119 (2013).

[184] J. Liu, D.A. Sonshine, S. Shervani, and R.H. Hurt, ACS Nano **4**, 6903 (2010).

[185] H.W. Choi, R.H. Dauskardt, S.C. Lee, K.R. Lee, and K.H. Oh, Diam. Relat. Mater. **17**, 252 (2008).

[186] K. Baba, R. Hatada, S. Flege, W. Ensinger, Y. Shibata, J. Nakashima, T. Sawase, and T. Morimura, in *Vacuum* (Pergamon, 2013), pp. 179–184.

[187] W.C. Lan, S.F. Ou, M.H. Lin, K.L. Ou, and M.Y. Tsai, Ceram. Int. **39**, 4099 (2013).

[188] R. Hatada, S. Flege, A. Bobrich, W. Ensinger, C. Dietz, K. Baba, T. Sawase, T. Watamoto, and T. Matsutani, Appl. Surf. Sci. **310**, 257 (2014).

[189] M. Cloutier, R. Tolouei, O. Lesage, L. Lévesque, S. Turgeon, M. Tatoulian, and D. Mantovani, Biointerphases **9**, 029013 (2014).

[190] T. Juknius, M. Ružauskas, T. Tamulevičius, R. Šiugždinienė, I. Juknienė, A. Vasiliauskas, A. Jurkevičiūtė, and S. Tamulevičius, Materials (Basel). **9**, 371 (2016).

[191] L. Swiatek, A. Olejnik, J. Grabarczyk, A. Jedrzejczak, A. Sobczyk-Guzenda, M. Kaminska, W. Jakubowski, W. Szymanski, and D. Bociaga, Diam. Relat. Mater. **67**, 54 (2016).

[192] G. Zakarienė, A. Novoslavskij, Š. Meškinis, A. Vasiliauskas, A. Tamulevičienė, S. Tamulevičius, T. Alter, and M. Malakauskas, Diam. Relat. Mater. **81**, 118 (2018).

[193] M. Janusz, L. Major, M. Kot, M. Dyner, J.M. Lackner, and B. Major, Biotribology **13**, 16 (2018).

[194] N.K. Manninen, S. V. Calderon, I. Carvalho, M. Henriques, A. Cavaleiro, and S. Carvalho, Appl. Surf. Sci. **377**, 283 (2016).

[195] L.J. Wang, F. Zhang, A. Fong, K.M. Lai, P.W. Shum, Z.F. Zhou, Z.F. Gao, and T. Fu, Thin Solid Films **650**, 58 (2018).

[196] R. Almaguer-Flores, Argelia; E-Rodil, Sandra; Olivares-Navarrete, (2011).

[197] D. Bociaga, P. Komorowski, D. Batory, W. Szymanski, A. Olejnik, K. Jastrzebski, and W. Jakubowski, Appl. Surf. Sci. **355**, (2015).

[198] D. Bociaga, W. Jakubowski, P. Komorowski, A. Sobczyk-Guzenda, A. Jędrzejczak, D. Batory, and A. Olejnik, Mater. Sci. Eng. C **63**, 462 (2016).

[199] F.P. Schwarz, I. Hauser-Gerspach, T. Waltimo, and B. Stritzker, Surf. Coatings Technol. **205**, 4850 (2011).

[200] N. Harrasser, S. Jüssen, I.J. Banke, R. Kmeth, R. von Eisenhart-Rothe, B. Stritzker, H. Gollwitzer, and R. Burgkart, AMB Express **5**, 1 (2015).

[201] C. Gorzelanny, R. Kmeth, A. Obermeier, A.T. Bauer, N. Halter, K. Kümpel, M.F. Schneider, A. Wixforth, H. Gollwitzer, R. Burgkart, B. Stritzker, and S.W. Schneider, Sci. Rep. **6**, 1 (2016).

[202] N. Harrasser, S. Jüssen, I.J. Banke, R. Kmeth, R. von Eisenhart-Rothe, B. Stritzker, H. Gollwitzer, and R. Burgkart, AMB Express **5**, (2015).

[203] N. Harrasser, S. Jüssen, A. Obermeir, R. Kmeth, B. Stritzker, H. Gollwitzer, and R. Burgkart, Biomater. Res. **20**, 1 (2016).

[204] A. Mazare, A. Anghel, C. Surdu-Bob, G. Totea, I. Demetrescu, and D. Ionita, Thin Solid Films **657**, 16 (2018).

[205] F.R. Marciano, L.F. Bonetti, L. V. Santos, N.S. Da-Silva, E.J. Corat, and V.J. Trava-Airoldi, Diam. Relat. Mater. **18**, 1010 (2009).

[206] J.L. Endrino, M. Allen, R.E. Galindo, H. Zhang, A. Anders, and J.M. Albella, in *Mater. Res. Soc. Symp. Proc.* (Materials Research Society, 2006), pp. 105–111.

[207] J.L. Endrino, R. Escobar Galindo, H.S. Zhang, M. Allen, R. Gago, A. Espinosa, and A. Anders, Surf. Coatings Technol. **202**, 3675 (2008).

[208] J.L. Endrino, A. Anders, J.M. Albella, J.A. Horton, T.H. Horton, P.R. Ayyalasomayajula, and M. Allen, in *J. Phys. Conf. Ser.* (Institute of Physics Publishing, 2010), p. 012012.

[209] S.C.H. Kwok, W. Zhang, G.J. Wan, D.R. McKenzie, M.M.M. Bilek, and P.K. Chu, Diam. Relat. Mater. **16**, (2007).

[210] N.M. Chekan, N.M. Beliauski, V. V. Akulich, L. V. Pozdniak, E.K. Sergeeva, A.N. Chernov, V. V. Kazbanov, and V.A. Kulchitsky, Diam. Relat. Mater. **18**, 1006 (2009).

[211] R.J. Narayan, H. Wang, and A. Tiwari, in *Mater. Res. Soc. Symp. - Proc.* (Materials Research Society, 2002), pp. 205–210.

[212] M.L. Morrison, R.A. Buchanan, P.K. Liaw, C.J. Berry, R.L. Brigmon, L. Riester, H. Abernathy, C. Jin, and R.J. Narayan, Diam. Relat. Mater. **15**, (2006).

[213] I.N. Mihailescu, D. Bociaga, G. Socol, G.E. Stan, M.C. Chifiriuc, C. Bleotu, M.A. Husanu, G. Popescu-Pelin, L. Duta, C.R. Luculescu, I. Negut, C. Hapenciuc, C. Besleaga, I. Zgura, and F. Miculescu, Int. J. Pharm. **515**, 592 (2016).

[214] P. Písařík, M. Jelínek, J. Remsa, J. Mikšovský, J. Zemek, K. Jurek, Kubinová, J. Lukeš, and J. Šepitka, Mater. Sci. Eng. C **77**, 955 (2017).

[215] L. Duta, C. Ristoscu, G.E. Stan, M.A. Husanu, C. Besleaga, M.C. Chifiriuc, V. Lazar, C. Bleotu, F. Miculescu, N. Mihailescu, E. Axente, M. Badiceanu, D. Bociaga, and I.N. Mihailescu, Appl. Surf. Sci. **441**, 871 (2018).

[216] H. Morisaki and H. Tabuchi, Colloids Surfaces B Biointerfaces **74**, 51 (2009).

[217] F. Hamadi, H. Latrache, M. Mabrrouki, A. Elghmari, A. Outzourhit, M. Ellouali, and A. Chtaini, J. Adhes. Sci. Technol. **19**, 73 (2005).

[218] T.R. Garrett, M. Bhakoo, and Z. Zhang, Prog. Nat. Sci. **18**, 1049 (2008).

[219] A.A.G. Bruzzone, H.L. Costa, P.M. Lonardo, and D.A. Lucca, CIRP Ann. - Manuf. Technol. **57**, 750 (2008).

[220] D. Mijatovic, J.C.T. Eijkel, and A. Van Den Berg, Lab Chip **5**, 492 (2005).

[221] A. Biswas, I.S. Bayer, A.S. Biris, T. Wang, E. Dervishi, and F. Faupel, Adv. Colloid Interface Sci. **170**, 2 (2012).

[222] S. Goel, M. Knaggs, G. Goel, X.W. Zhou, H.M. Upadhyaya, V.K. Thakur, V. Kumar, G. Bizarri, A. Tiwari, A. Murphy, A. Stukowski, and A. Matthews, Mater. Today Chem. **18**, 100356 (2020).

[223] K. Das, S. Bose, and A. Bandyopadhyay, Acta Biomater. **3**, (2007).

[224] J. Gopal, R.P. George, P. Muraleedharan, and H.S. Khatak, Biofouling **20**, 167 (2004).

[225] B. Ercan, K.M. Kummer, K.M. Tarquinio, and T.J. Webster, Acta Biomater. **7**, 3003 (2011).

[226] A. Bendavid, P.J. Martin, L. Randeniya, and M.S. Amin, Diam. Relat. Mater. **18**, 66 (2009).

[227] O. Santos, T. Nylander, R. Rosmaninho, G. Rizzo, S. Yiantsios, N. Andritsos, A. Karabelas, H. Müller-Steinhagen, L. Melo, L. Boulangé-Petermann, C. Gabet, A. Braem, C. Trägårdh, and M. Paulsson, J. Food Eng. **64**, (2004).

[228] Y.-Y. Zhao, B. Zhao, X. Su, S. Zhang, S. Wang, R. Keatch, and Q. Zhao, Biofouling **34**, 26 (2018).

[229] A. Ewald, S.K. Glückermann, R. Thull, and U. Gbureck, Biomed. Eng. Online **5**, 22 (2006).

[230] K.C. Park, H.J. Choi, C.H. Chang, R.E. Cohen, G.H. McKinley, and G. Barbastathis, ACS Nano **6**, 3789 (2012).

[231] T.R. Rautray, R. Narayanan, and K.H. Kim, Prog. Mater. Sci. **56**, 1137 (2011).

[232] P. Brunette, D.M; Tengvall, Pentti; Textor, Marcus-Hans; Thomsen, (2012).

[233] J. Xu, G. Ding, J. Li, S. Yang, B. Fang, H. Sun, and Y. Zhou, Appl. Surf. Sci. **256**, 7540 (2010).

[234] S. Mändl, R. Sader, G. Thorwarth, D. Krause, H.F. Zeilhofer, H.H. Horch, and B. Rauschenbach, in *Biomol. Eng.* (2002).

[235] M.N. Dickson, E.I. Liang, L.A. Rodriguez, N. Vollereaux, and A.F. Yee, Biointerphases **10**, 021010 (2015).

[236] S. Wu, F. Zuber, J. Brugger, K. Maniura-Weber, and Q. Ren, Nanoscale **8**, 2620 (2016).

[237] L.G. Harris, S. Tosatti, M. Wieland, M. Textor, and R.G. Richards, Biomaterials **25**, (2004).

[238] W.-H. Kim, S.-B. Lee, K.-T. Oh, S.-K. Moon, K.-M. Kim, and K.-N. Kim, Surf. Interface Anal. **40**, 202 (2008).

[239] K.C. Popat, M. Eltgroth, T.J. LaTempa, C.A. Grimes, and T.A. Desai, Biomaterials **28**, (2007).

[240] C.R. Crick, S. Ismail, J. Pratten, and I.P. Parkin, Thin Solid Films **519**, 3722 (2011).

[241] L. Li, M. Hong, M. Schmidt, M. Zhong, A. Malshe, B. Huis In'Tveld, and V. Kovalenko, CIRP Ann. - Manuf. Technol. **60**, 735 (2011).

[242] J. Dutta Majumdar and I. Manna, Sadhana - Acad. Proc. Eng. Sci. **28**, 495 (2003).

[243] T.N. Baker, in *Surf. Eng. Light Alloy. Alum. Magnes. Titan. Alloy.* (2010).

[244] T.L. See, [Thesis]. Manchester, UK Univ. Manchester; 2015. (2015).

[245] F.C. Burns and S.R. Cain, J. Phys. D. Appl. Phys. **29**, 1349 (1996).

[246] M.P. Fiorucci, A.J. López, and A. Ramil, Int. J. Adv. Manuf. Technol. **75**, 515 (2014).

[247] B.N. Chichkov, C. Momma, S. Nolte, F. Von Alvensleben, and A. Tünnermann, Appl. Phys. A Mater. Sci. Process. **63**, 109 (1996).

[248] H. Reimers, J. Gold, B. Kasemo, and D. Chakarov, Appl. Phys. A Mater. Sci. Process. **77**, 491 (2003).

[249] F.J.C. Braga, R.F.C. Marques, E. de A. Filho, and A.C. Guastaldi, Appl. Surf. Sci. **253**, 9203 (2007).

[250] M. Trtica, B. Gakovic, D. Batani, T. Desai, P. Panjan, and B. Radak, Appl. Surf. Sci. **253**, (2006).

[251] B.K. Nayak, M.C. Gupta, and K.W. Kolasinski, Appl. Phys. A, **90**, 399 (2008).

[252] W.O. Soboyejo, C. Mercer, S. Allameh, B. Nemetski, N. Marcantonio, and J.L. Ricci, Key Eng. Mater. **198**–**199**, 203 (2001).

[253] S. Shaikh, S. Kedia, D. Singh, M. Subramanian, and S. Sinha, J. Laser Appl. **31**, 022011 (2019).

[254] J. Chen, S. Mwenifumbo, C. Langhammer, J.-P. McGovern, M. Li, A. Beye, and W.O. Soboyejo, J. Biomed. Mater. Res. Part B Appl. Biomater. **82B**, 360 (2007).

[255] A.Y. Fasasi, S. Mwenifumbo, N. Rahbar, J. Chen, M. Li, A.C. Beye, C.B. Arnold, and W.O. Soboyejo, Mater. Sci. Eng. C **29**, 5 (2009).

[256] A.C. Duncan, F. Weisbuch, F. Rouais, S. Lazare, and C. Baquey, Biosens. Bioelectron. **17**, (2002).

[257] L. Giner, M. Mercadé, S. Torrent, M. Punset, R.A. Pérez, L.M. Delgado, and F.J. Gil, J. Appl. Biomater. Funct. Mater. **16**, 83 (2018).

[258] S. Zinelis, Dent. Mater. **23**, (2007).

[259] A.K. Geim, S. V. Dubonos, I. V. Grigorieva, K.S. Novoselov, A.A. Zhukov, and S.Y. Shapoval, Nat. Mater. **2**, (2003).

[260] S. Latthe, C. Terashima, K. Nakata, and A. Fujishima, Molecules **19**, 4256 (2014).

[261] D. Patil, S. Aravindan, M.K. Wasson, P. Vivekanandan, and P. V. Rao, J. Micro Nano-Manufacturing **6**, (2018).

[262] R. Bürgers, T. Gerlach, S. Hahnel, F. Schwarz, G. Handel, and M. Gosau, Clin. Oral Implants Res. **21**, 156 (2010).

[263] F. Variola, S.F. Zalzal, A. Leduc, J. Barbeau, and A. Nanci, Int. J. Nanomedicine **9**, 2319 (2014).

[264] D.J. Balazs, K. Triandafillu, Y. Chevolot, B.-O. Aronsson, H. Harms, P. Descouts, and H.J. Mathieu, Surf. Interface Anal. **35**, 301 (2003).

[265] C. Serrano, L. García-Fernández, J.P. Fernández-Blázquez, M. Barbeck, S. Ghanaati, R. Unger, J. Kirkpatrick, E. Arzt, L. Funk, P. Turón, and A. del Campo, Biomaterials **52**, 291 (2015).

[266] B. Bhushan, *Springer Handbook of Nanotechnology*, 4th ed. (Springer, 2017).

[267] R. Jiang, L. Hao, L. Song, L. Tian, Y. Fan, J. Zhao, C. Liu, W. Ming, and L. Ren, Chem. Eng. J. **398**, 125609 (2020).

[268] X.-Q. Liu, Q.-D. Chen, R. Wang, L. Wang, X.-L. Yu, J.-N. Cao, Y.-M. Zhou, and H.-B. Sun, Adv. Mater. Interfaces **2**, 1500058 (2015).

[269] D. V. Ta, A. Dunn, T.J. Wasley, R.W. Kay, J. Stringer, P.J. Smith, C. Connaughton, and J.D. Shephard, Appl. Surf. Sci. **357**, 248 (2015).

[270] R. Leach, *Optical Measurement of Surface Topography* (2011).

[271] M. Quinten, in (Springer, Cham, 2019), pp. 67–93.

[272] H. Villarraga-Gómez, L. Körner, R. Leach, and S.T. Smith, Precis. Eng. **64**, 228 (2020).

[273] S. Rosén, T.R. Thomas, and B.G. Rosén, Surf. Topogr. Metrol. Prop. **2**, 014005 (2014).

[274] K. Stout and L. Blunt, *Three Dimensional Surface Topography*, 2nd ed. (Elsevier, 2000).